

MIT Open Access Articles

Protracted timescales of lower crustal growth at the fast-spreading East Pacific Rise

The MIT Faculty has made this article openly available. **Please share** how this access benefits you. Your story matters.

Citation: Rioux, Matthew, C. Johan Lissenberg, Noah M. McLean, Samuel A. Bowring, Christopher J. MacLeod, Eric Hellebrand, and Nobumichi Shimizu. "Protracted Timescales of Lower Crustal Growth at the Fast-Spreading East Pacific Rise." *Nature Geoscience* 5, no. 4 (January 29, 2012): 275–278.

As Published: <http://dx.doi.org/10.1038/ngeo1378>

Publisher: Nature Publishing Group

Persistent URL: <http://hdl.handle.net/1721.1/85184>

Version: Author's final manuscript: final author's manuscript post peer review, without publisher's formatting or copy editing

Terms of use: Creative Commons Attribution-Noncommercial-Share Alike



Protracted time scales of lower crustal growth at the fast-spreading East Pacific Rise

Matthew Rioux^{1*}, C. Johan Lissenberg², Noah M. McLean¹, Samuel A. Bowring¹, Christopher J. MacLeod², Eric Hellebrand³, Nobumichi Shimizu⁴

¹Department of Earth, Atmospheric, and Planetary Sciences, Massachusetts Institute of Technology, Cambridge, MA 02459, USA

²School of Earth and Ocean Sciences, Cardiff University, Cardiff, CF10 3AT, United Kingdom

³Department of Geology and Geophysics, University of Hawaii, Honolulu, HI 96822, USA

⁴Woods Hole Oceanographic Institution, Woods Hole, MA 02543, USA

*Corresponding author. e-mail: riouxm@mit.edu

Formation of the oceanic crust at mid-ocean ridges is a fundamental component of plate tectonics. A majority of the crust at many ridges is composed of plutonic rocks that form by crystallization of mantle-derived magmas within the crust. Recent application of U/Pb dating to samples from in-situ oceanic crust has begun to provide exciting new insight into the timing, duration and distribution of magmatism during formation of the plutonic crust¹⁻⁴. Previous studies have focused on samples from slow-spreading ridges, however, the time scales and processes of crustal growth are expected to vary with plate spreading rate. Here we present the first high-precision dates from plutonic crust formed at the fast-spreading East Pacific Rise (EPR). Individual zircon minerals yielded dates from 1.420–1.271 million years ago, with uncertainties of ± 0.006 – 0.081 million years. Within individual samples, zircons record a range of dates of up to ~ 0.124 million years, consistent with protracted crystallization or assimilation of older zircons from adjacent rocks. The variability in dates is comparable to data from the Vema lithospheric section on the Mid-Atlantic Ridge (MAR)³, suggesting that time scales of magmatic processes in the lower crust may be similar at slow- and fast-spreading ridges.

Seismic reflection data suggest that fast-spreading ridges are typically underlain by small axial melt lenses that are <100 m high, 0.5-1.0 km wide and are located ~ 1 – 1.5 km below the seafloor⁵⁻⁷. Seismic refraction and sea floor compliance studies indicate that the melt lenses overlie broader low velocity zones that are interpreted as regions of high temperature crust containing low degrees of partial melt^{8,9}. A second melt lens has also been identified at Moho depths in some studies⁹. The purpose of this study was to constrain the timescales of magmatic processes within an upper melt lens and mush zone beneath the fast-spreading EPR.

The dated samples were collected from lower crustal exposures in Hess Deep, a bathymetric low (5400 mbsl) located along the southern margin of the Cocos plate, at the junction of the Pacific, Cocos and Nazca plates in the eastern Pacific Ocean¹⁰ ($\sim 2^\circ\text{N}$; Figure 1). The junction between the three plates is partitioned into three triple junctions on the margins of the Galapagos microplate¹¹. Hess Deep formed as a result of rifting associated with propagation of the Cocos-Nazca ridge into crust formed at the EPR¹². The northern and southern boundaries of the rift valley are defined by major normal fault scarps that expose upper levels of EPR crust, including pillow basalts, sheeted dikes and isotropic gabbros¹³. An east-west trending intra-rift ridge, located along the northern margin of the rift basin, exposes a faulted cross section through EPR crust and uppermost mantle, from sheeted dikes to mantle peridotite^{14,15} (Figure 1). Basalts from the Cocos-Nazca spreading ridge are found on the floor of the rift basin.

The analyzed zircons were separated from four isotropic gabbro and gabbro-norite samples from the western end of the intra-rift ridge (Supplementary Data, Supplementary Figure 1). The samples were collected in 2008 by the *Isis* ROV during RRS *James Cook* cruise JC21¹⁶ (Figure 1, Supplementary Table 1) and are from outcrops at two different dive localities, in the upper part of the plutonic section. Our stratigraphic reconstructions indicate that the 78R samples come from ~ 120 m below the dike-gabbro transition, whereas the 76R sample comes from ~ 1300 m below the transition. The two dives were also separated laterally, with the 76R dive located 1.1 km west of the 78R dive. Whole rock and mineral geochemical data indicate that all of the dated gabbros and

gabbro-norites are evolved cumulates that experienced post-cumulus flow of evolved and trace element enriched melts¹⁷.

We dated 54 zircons from the four samples using isotope dilution-thermal ionization mass spectrometry (ID-TIMS). Cathodoluminescence (CL) images and Y and Hf maps were used to characterize the zoning and structure of zircons in each sample. The data reveal un-zoned, sector zoned and oscillatory zoned grains (Figure 2, Supplementary Figure 2). In addition, several grains from JC21-78R-5 contain core regions overgrown by rims. The dated grains include grains that were first imaged and then removed from the mounts, and un-imaged whole grains and grain fragments.

Single grain and grain fragment $^{206}\text{Pb}/^{238}\text{U}$ dates from the four samples range from 1.420–1.271 Ma, with 2σ uncertainties of ± 0.006 – 0.081 Ma (Figure 3, Supplementary Methods, Supplementary Table 2). The data were corrected for initial exclusion of ^{230}Th , which results in secular disequilibrium in the ^{238}U decay chain, assuming a constant magma Th/U estimated from existing isotope dilution Th/U measurements of basaltic glasses from the EPR (Th/U = 2.23 ± 0.31 ; 2σ). Weighted mean statistics are a useful way to analyze whether the distribution of dates within individual samples reflect analytical uncertainties or resolvable dispersion in the zircon crystallization ages. To determine whether the observed scatter can be explained by analytical uncertainties alone, the mean square of the weighted deviates¹⁸ (MSWD) of the weighted mean, more widely known as the reduced chi-squared statistic, is often calculated. A MSWD ≈ 1 suggests that, within analytical uncertainties, the data are consistent with a null hypothesis that all zircons crystallized synchronously. Conversely, if the two-sided p-value for the chi-squared goodness of fit is ≤ 0.05 (i.e., MSWD $\gg 1$), we reject the null hypothesis, suggesting resolvable scatter in the crystallization ages.

Samples JC21-76R-4 and JC21-78R-2 have weighted mean MSWD consistent with measurement of a homogeneous population of zircon dates. In contrast, samples JC21-78R-1 and JC21-78R-5 have MSWD of 2.3 ($n = 15$) and 4.0 ($n = 14$) and two sided p-values ≤ 0.05 , implying resolvable age variations. To quantify the variability within these samples, we calculated the overdispersion beyond analytical uncertainties using the maximum likelihood estimate of Vermeesch¹⁹. This approach models the observed dispersion in ^{230}Th -corrected zircon dates as the result of analytical scatter about a parent Gaussian distribution of true crystallization ages, instead of assuming the data represent repeat measurements of a single true crystallization age. We report the overdispersion parameter as the length of the $\sim 95\%$ confidence interval (4ξ) of the estimated parent distribution, with the 2σ absolute standard error of this value. Although the shape of the distribution of crystallization dates is unknown, a Gaussian is a reasonable approximation. Samples JC21-78R-1 and JC21-78R-5 have calculated overdispersion parameters of 0.047 ± 0.009 Ma and 0.124 ± 0.016 Ma, respectively. The observed variability in single grain dates provides a minimum estimate for the range of zircon crystallization ages because the grain fragment and single grain analyses may average core and rim ages in complex grains.

The absolute dates and the overdispersion of the data within individual samples are sensitive to the Th-correction applied (Supplementary Figure 3, Supplementary Table 2). Application of a variety of end member Th-correction models generates small displacements in the Th-corrected $^{206}\text{Pb}/^{238}\text{U}$ dates, but always results in resolvable

overdispersions (Supplementary Methods). Therefore, we are confident that our conclusions are independent of the correction for initial Th disequilibrium.

The U/Pb dates provide direct constraints on the time scales of magmatic evolution beneath the EPR. The overdispersion in the $^{206}\text{Pb}/^{238}\text{U}$ dates within individual samples could reflect protracted crystallization of a single magmatic pulse, repeated recharge of a magma chamber or mush zone, or assimilation of older zircon during anatexis of adjacent wall rocks; it is not possible to differentiate between these models based on the current data. The evidence for discrete cores and rims in CL images and chemical maps of zircons from JC21-78R-5 may reflect the protracted magmatic history for this sample (Figure 2, Supplementary Figure 2). However, we were unable to date any of the imaged grains with discrete cores because they did not contain enough radiogenic Pb, and therefore we could not directly test the relationship between zircon structure and date.

The 78R samples occur at the same depth as the axial melt lenses present below modern fast-spreading ridges^{5,7} and may represent the crystallized equivalent of the melt lens (e.g.,²⁰). The 76R sample comes from a depth that is within the low-velocity zone at modern ridges^{8,9}. The $^{206}\text{Pb}/^{238}\text{U}$ dates from the two dive localities overlap, suggesting that magmas were crystallizing simultaneously at variable depths in the crust, within the resolution of our analytical uncertainties. The $^{206}\text{Pb}/^{238}\text{U}$ dates are consistent with the spreading rate at this latitude calculated from magnetic data²¹ and the tectonic history of Hess Deep¹¹ (Supplementary Discussion).

The observed 0.12 Ma growth history in JC21-78R-5 corresponds to ~8 km of spreading at this latitude on the EPR²¹ (half rate), which is greater than the full width of geophysically imaged axial melt lenses⁷ (~0.5–1.0 km wide) or mush zones^{8,9} (~5–7 km) beneath the modern rise. However, $^{226}\text{Ra}/^{230}\text{Th}$ disequilibrium in some EPR samples suggest that volcanism may extend up to 20 km from the rise axis²². Further, seismic data from ~9°20'N on the EPR is consistent with a thin melt lens 20 km off axis, which may be related to the axis of mantle upwelling being offset from the ridge axis in this area²³. Seismic reflectivity data from overlapping spreading centers at 9°03'N on the EPR also suggest that axial discontinuities can be underlain by a wide and complex distribution of melt²⁴. A similar axial discontinuity is located at ~2°N on the EPR, southwest of Hess Deep. The extended growth history of the analyzed EPR zircons may therefore reflect either continued magmatic activity beyond the width of seismically imaged melt lenses/mush zones or formation in an anomalously wide magmatic zone.

Comparison of the new results from Hess Deep to earlier U/Pb zircon dating from the lower crust at slow spreading ridges, provides a context for the new dates and their implications for mid-ocean ridge processes. Lissenberg et al.³ presented high-precision ID-TIMS single grain and grain fragment zircon dates from five oxide-bearing gabbros collected from the Vema lithospheric section at 11°N on the MAR. Single grain $^{206}\text{Pb}/^{238}\text{U}$ dates ranged from 13.71–13.24 Ma, with uncertainties of 0.012–0.20 Ma (Supplementary Figure 4, Supplementary Table 3; data recalculated using the new U/Pb_Redux algorithms and a revised estimate of the laboratory blank isotopic composition, which were not available when the data were originally published). One of the five samples has a weighted mean MSWD consistent with a single population, within the resolution of the analytical uncertainties. The four other samples have calculated overdispersion

parameters of 0.078 ± 0.016 Ma, 0.104 ± 0.033 Ma, 0.150 ± 0.038 Ma, and 0.166 ± 0.045 Ma.

Lower precision sensitive high resolution ion microprobe (SHRIMP) $^{206}\text{Pb}/^{238}\text{U}$ zircon dates from Atlantis Massif (MAR) record similar to slightly larger intra-sample variations: 4 of 16 analyzed samples have weighted mean MSWDs that are higher than expected for a single zircon population and have overdispersion parameters of 0.169 ± 0.032 Ma to 0.298 ± 0.054 Ma² (two sample with porous zircon were excluded from the calculations). Other SHRIMP studies have focused on older samples from the Southwest Indian Ridge (SWIR) and the absolute uncertainties are too large to resolve 0.1–0.2 Ma variations^{1,4}. Comparison of the overdispersion in TIMS versus SHRIMP data may be biased by differences in analytical procedures, data reduction and error propagation, and we consider the direct comparison between the high-precision TIMS data from the EPR and Vema samples to be the most robust.

The similarity in the overdispersion of zircon dates in the Hess Deep and Vema samples (Figure 2, Supplementary Figures 3 and 4) is surprising given the significant differences in spreading rate between the MAR and EPR, and the associated contrast in the inferred thermal conditions and structure of the crust and upper mantle. The duration of zircon crystallization is likely to reflect a balance between spreading rate, magma supply and thermal structure. Fast-spreading ridges are characterized by high magmatic fluxes and higher crustal temperatures, potentially facilitating stable long-lived magmatic centers and protracted zircon crystallization. However, newly formed crust is rapidly transported away from the ridge axis (~ 75 m/ka), restricting the opportunity for interaction between successive magmatic pulses or between axial magmas and older crust. This may limit the duration of zircon growth and prevent inheritance of significantly older xenocrystic zircons. Off-axis magmatism (e.g., ²²) or broadening of the melt lens/mush zone^{23,24} could extend the duration of zircon crystallization or increase the potential for interaction with older crustal material in some areas.

In contrast, slow-spreading ridges are characterized by lower magma supply and lower crustal temperatures, which could lead to more rapid crystallization. However, on average, crust remains within the zone of axial magmatism for longer periods of time, increasing the possibility that magmas will be recharged by subsequent magmatic pulses or inherit older zircon from adjacent wall rocks. Thick axial lithosphere at slow-spreading ridges may also result in variable crystallization depths, with some magmas beginning to crystallize in the mantle²⁵: a process that has been evoked to explain anomalously old U/Pb zircon dates from the SWIR and MAR^{2,4}. The similar dispersion of zircon crystallization dates in the Hess Deep and Vema samples may therefore reflect a balance between a range of competing parameters at different spreading rates. Additional studies are needed to determine whether the data from Hess Deep and Vema are representative of the global mid-ocean ridge system, and to provide a more robust comparison between different spreading rates, intrusion depths and crustal structures.

Methods

High-precision single grain and grain fragment U/Pb zircon analyses were carried out in the radiogenic isotope laboratory at the Massachusetts Institute of Technology (MIT). Grains were dissolved in two-steps following the chemical abrasion method²⁶, which isolates the lower uranium portions of the grains and thus minimizes the impact of post-

magmatic Pb loss related to radiation damage. U/Pb isotopic ratios were determined by ID-TIMS. The analyzed zircons contained low amounts of radiogenic Pb (0.06–1.4 pg), which increased the importance of minimizing and accurately correcting for laboratory Pb blanks ($Pb_c = 0.17\text{--}0.70$ pg). Data were reduced using the U/Pb_Redux software package^{27,28}. Hf and Y concentration maps and cathodoluminescence (CL) and backscatter (BSE) images were collected on the JEOL Hyperprobe JXA-8500F at the University of Hawaii and the JEOL Superprobe JXA-733 at MIT (Supplementary Figure 2). Analytical procedures, U/Pb isotopic data and a detailed discussion of the impact of different Th-correction models are given in the Supplementary Methods.

References

- 1 Baines, A. G. *et al.* SHRIMP Pb/U zircon ages constrain gabbroic crustal accretion at Atlantis Bank on the ultraslow-spreading Southwest Indian Ridge. *Earth and Planet. Sci. Let.* **287**, 540-550 (2009).
- 2 Grimes, C. B., John, B. E., Cheadle, M. J. & Wooden, J. L. Protracted construction of gabbroic crust at a slow spreading ridge: Constraints from ²⁰⁶Pb/²³⁸U zircon ages from Atlantis Massif and IODP Hole U1309D (30°N, MAR). *Geochem. Geophys. Geosyst.* **9**, Q08012 (2008).
- 3 Lissenberg, C. J., Rioux, M., Shimizu, N., Bowring, S. A. & Mevel, C. Zircon dating of oceanic crustal accretion. *Science* **323**, 1048-1050 (2009).
- 4 Schwartz, J. J. *et al.* Dating the growth of oceanic crust at a slow-spreading ridge. *Science* **310**, 654-657 (2005).
- 5 Detrick, R. S. *et al.* Multi-channel seismic imaging of a crustal magma chamber along the East Pacific Rise. *Nature* **326**, 35-41 (1987).
- 6 Hussenoeder, S. A., Collins, J. A., Kent, G. M., Detrick, R. S. & the, T. G. Seismic analysis of the axial magma chamber reflector along the southern East Pacific Rise from conventional reflection profiling. *J. Geophys. Res.* **101**, 22087-22105 (1996).
- 7 Hooft, E. E. E., Detrick, R. S. & Kent, G. M. Seismic structure and indicators of magma budget along the Southern East Pacific Rise. *J. Geophys. Res.* **102**, 27319-27340 (1997).
- 8 Dunn, R. A., Toomey, D. R. & Solomon, S. C. Three-dimensional seismic structure and physical properties of the crust and shallow mantle beneath the East Pacific Rise at 9°30'N. *J. Geophys. Res.* **105**, 23537-23555 (2000).
- 9 Crawford, W. C. & Webb, S. C. Variations in the distribution of magma in the lower crust and at the Moho beneath the East Pacific Rise at 9°–10°N. *Earth and Planet. Sci. Let.* **203**, 117-130 (2002).
- 10 Hey, R. N., Deffeyes, K. S., Johnson, G. L. & Lowrie, A. The Galapagos Triple Junction and plate motions in the East Pacific. *Nature* **237**, 20-22 (1972).
- 11 Lonsdale, P. Structural pattern of the Galapagos Microplate and evolution of the Galapagos Triple Junctions. *J. Geophys. Res.* **93**, 13551-13574 (1988).
- 12 Lonsdale, P. Regional shape and tectonics of the equatorial East Pacific Rise. *Mar. Geophys. Res.* **3**, 295-315 (1977).
- 13 Karson, J. A. *et al.* Structure of uppermost fast-spread oceanic crust exposed at the Hess Deep Rift: Implications for subaxial processes at the East Pacific Rise. *Geochem. Geophys. Geosyst.* **3**, 2001GC000155 (2002).

- 14 Francheteau, J. *et al.* 1 Ma East Pacific Rise oceanic crust and uppermost mantle exposed by rifting in Hess Deep (equatorial Pacific Ocean). *Earth and Planet. Sci. Let.* **101**, 281-295 (1990).
- 15 MacLeod, C. J., C  lerier, B., Fr  h-Green, G. L. & Manning, C. E. in *Proceedings of the Ocean Drilling Program, Scientific Results* Vol. 147 (eds C. M  vel, K. M. Gillis, J. F. Allan, & P.S. Meyer) (Ocean Drilling Program, 1996).
- 16 MacLeod, C. J., Teagle, D. A. H., Gillis, K. M., Shillington, D. J. & RRS James Cook Cruise JC21 Scientific Party. Morphotectonics of Hess Deep: Preliminary results of RRS James Cook Cruise JC21. *AGU Fall Meeting*, V43I-08 (2008).
- 17 Lissenberg, C. J., MacLeod, C. J., Howard, K. A. & Godard, M. Pervasive reactive melt migration through the lower oceanic crust. *AGU Fall Meeting*, V13F-02 (2011).
- 18 Wendt, I. & Carl, C. The statistical distribution of the mean squared weighted deviation. *Chem. Geol.* **86**, 275-285 (1991).
- 19 Vermeesch, P. HelioPlot, and the treatment of overdispersed (U-Th-Sm)/He data. *Chem. Geol.* **271**, 108-111 (2010).
- 20 MacLeod, C. J. & Yaouancq, G. A fossil melt lens in the Oman ophiolite: Implications for magma chamber processes at fast-spreading ridges. *Earth and Planet. Sci. Let.* **176**, 357-373 (2000).
- 21 DeMets, C., Gordon, R. G. & Argus, D. F. Geologically current plate motions. *Geophys. J. Int.* **181**, 1-80 (2010).
- 22 Turner, S., Beier, C., Niu, Y. & Cook, C. U-Th-Ra disequilibria and the extent of off-axis volcanism across the East Pacific Rise at 9  30'N, 10  30'N, and 11  20'N. *Geochem. Geophys. Geosyst.* **12**, Q0AC12 (2011).
- 23 Durant, D. T. & Toomey, D. R. Evidence and implications of crustal magmatism on the flanks of the East Pacific Rise. *Earth and Planet. Sci. Let.* **287**, 130-136 (2009).
- 24 Kent, G. M. *et al.* Evidence from three-dimensional seismic reflectivity images for enhanced melt supply beneath mid-ocean-ridge discontinuities. *Nature* **406**, 614-618 (2000).
- 25 Cannat, M. How thick is the magmatic crust at slow spreading oceanic ridges? *J. Geophys. Res.* **101**, 2847-2857 (1996).
- 26 Mattinson, J. M. Zircon U/Pb chemical abrasion (CA-TIMS) method: Combined annealing and multi-step partial dissolution analysis for improved precision and accuracy of zircon ages. *Chem. Geol.* **220**, 47-66 (2005).
- 27 Bowring, J. F., McLean, N. M. & Bowring, S. A. Engineering cyber infrastructure for U-Pb geochronology: Tripoli and U-Pb_Redux. *Geochem. Geophys. Geosyst.* **12**, Q0AA19 (2011).
- 28 McLean, N. M., Bowring, J. F. & Bowring, S. A. An algorithm for U-Pb isotope dilution data reduction and uncertainty propagation. *Geochem. Geophys. Geosyst.* **12**, Q0AA18 (2011).
- 29 Schouten, H., Smith, D. K., Mont  si, L. G. J., Zhu, W. & Klein, E. M. Cracking of lithosphere north of the Galapagos triple junction. *Geology* **36**, 339-342 (2008).
- 30 Smith, D. K., Schouten, H., Zhu, W.-l., Mont  si, L. G. J. & Cann, J. R. Distributed deformation ahead of the Cocos-Nazca Rift at the Galapagos triple junction. *Geochem. Geophys. Geosyst.* **12**, Q11003 (2011).

Acknowledgements

This research was partially funded by NSF grant OCE-0727914 (SAB), a Cardiff University International Collaboration Award (CJL) and NERC grant NE/C509023/1 (CJM). We thank Linnea Koons for separating the Hess Deep zircons, Oliver Jagoutz and Fred Frey for useful discussions of Th and U partitioning in zircon, and Doug Wilson for reading and commenting on a draft of the manuscript. We thank Joshua Schwartz and Graham Baines for detailed and useful reviews.

Figure Captions

Figure 1. Tectonic setting of Hess Deep. (a) Morphotectonic map of the Galapagos microplate region (after Lonsdale¹¹) incorporating data from RRS *James Cook* cruise JC21, Lonsdale¹¹, Schouten et al.²⁹, Smith et al.³⁰, and GeoMapApp (<http://www.geomapapp.org>). (b) Three dimensional perspective bathymetric map of Hess Deep showing the locations and lithologies of samples recovered by the *Isis* ROV during RRS *James Cook* cruise JC21. Dated samples are marked with stars. Inset map shows location of Hess Deep and regional tectonic setting (after Lonsdale¹¹). PP, Pacific Plate; CP, Cocos Plate; GP, Galapagos Plate; NP, Nazca Plate; C-N basalt, Cocos-Nazca basalt; Gabbro s.l., Gabbro sensu lato.

Figure 2. Representative zircon cathodoluminescence (CL) images. The images with grain numbers (i.e., z1) correspond to dated zircons. The white bar in each image is a 50 μm scale bar. Additional CL images and Y maps are provided in Supplementary Figure 2.

Figure 3. Single grain and grain fragment $^{206}\text{Pb}/^{238}\text{U}$ zircon dates from Hess Deep gabbro and gabbroonites. Data were Th-corrected assuming a constant magma Th/U = 2.23 ± 0.31 (2σ). Uncertainties are represented as 2σ confidence intervals. Overdispersion (ovds) in dates calculated following Vermeesch¹⁹.

Author Contributions

MR performed zircon geochronology and wrote the paper. CJL collected the samples, performed trace element analyses and generated CL and BSE images. NM provided statistical expertise. SAB assisted with zircon geochronology. CJM collected the samples and drafted the maps. EH generated Y and Hf maps and CL and BSE images. NS performed trace element analyses.

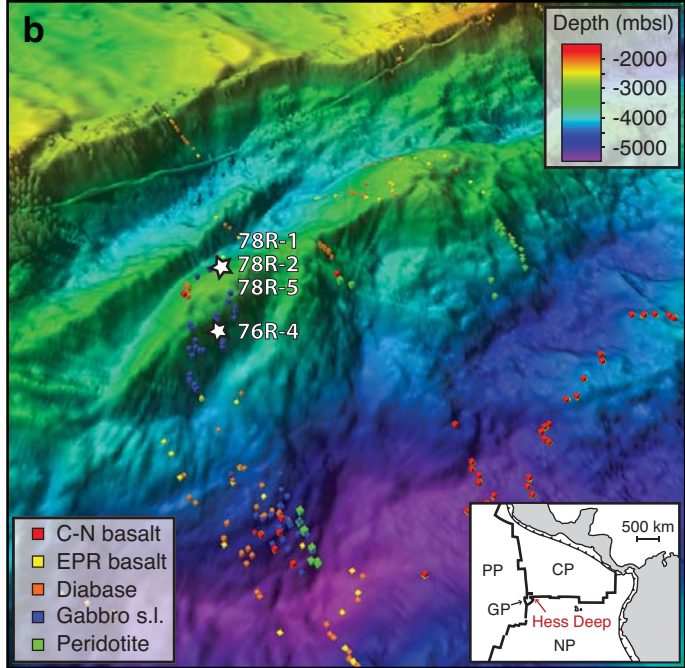
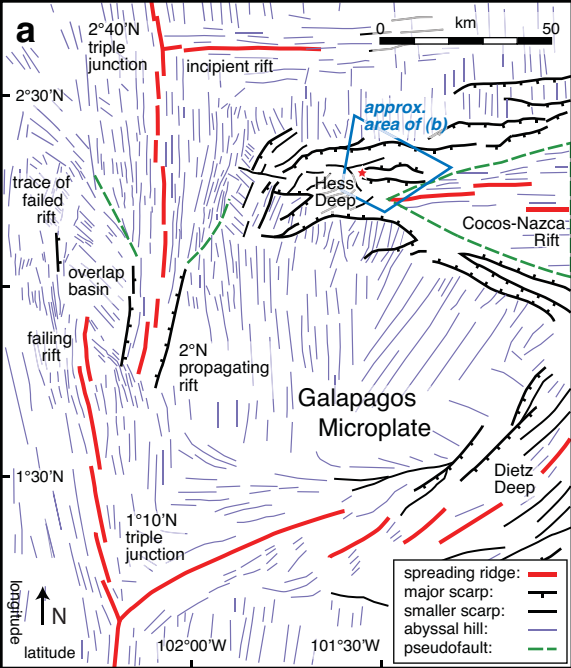
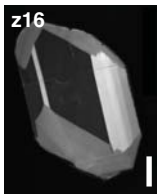
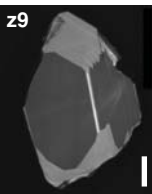
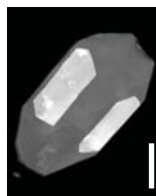
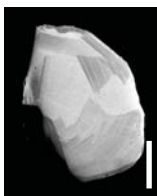
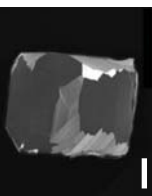
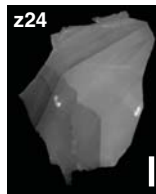
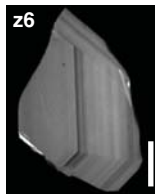


Figure 1

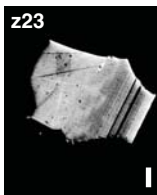
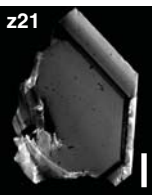
JC21-76R-4



JC21-78R-1



JC21-78R-2



JC21-78R-5

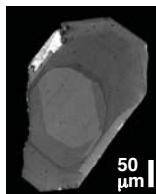
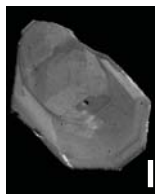
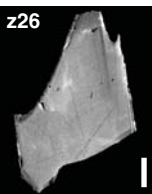
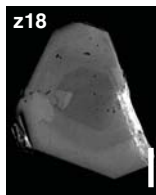
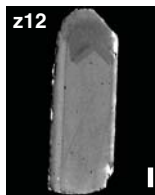


Figure 2

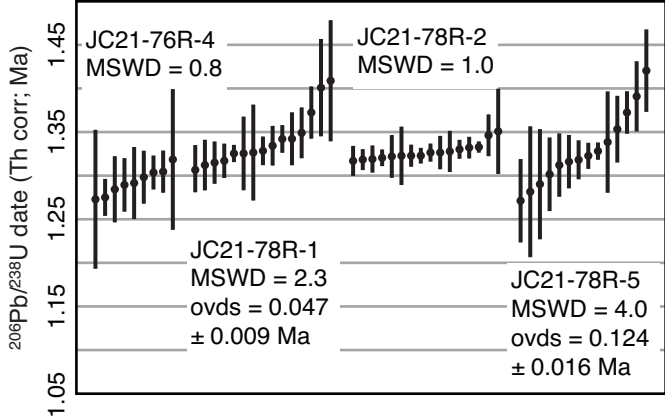


Figure 3

Protracted time scales of lower crustal growth at the fast-spreading East Pacific Rise

Matthew Rioux, C. Johan Lissenberg, Noah M. McLean, Samuel A. Bowring, Christopher J. MacLeod, Eric Hellebrand, Nobumichi Shimizu

Supplementary Data—Sample descriptions

JC21-76R-4: medium- to coarse-grained, equigranular, oxide-bearing gabbro (10% opx).

JC21-78R-1: medium-grained, equigranular, opx- and oxide bearing gabbro, with primary brown amphibole.

JC21-78R-2: medium- to coarse-grained, equigranular, opx-bearing oxide gabbro (10% oxides), with primary brown amphibole.

JC21-78R-5: medium- to coarse-grained varitextured rock, with domains ranging in composition from oxide gabbro to gabbro.

Supplementary Methods—U-Pb zircon geochronology

Single grain and grain fragment U-Pb zircon dates were determined by isotope dilution-thermal ionization mass spectrometry (ID-TIMS) at the Massachusetts Institute of Technology. Individual grains were annealed at 900°C for 60 hours and dissolved in two steps, following the chemical abrasion method¹ (CA-TIMS). Initial digestions were carried out in full strength HF in Parr acid digestion vessels held at 210°C for 12–14 hours. Grains were then rinsed in H₂O, sonicated and fluxed on a hot plate (~80°C) in ~7N HNO₃, re-rinsed in H₂O, and then re-loaded into micro-capsules. The samples were subsequently spiked with the EARTHTIME ²⁰⁵Pb-²³³U-²³⁵U tracer and dissolved in concentrated HF in Parr acid digestion vessels held at 220°C for 48–72 hours. Following digestion, the HF solutions were dried down, re-dissolved in 6.2N HCl and returned to a 180°C oven for 6–12 hours. Samples were then converted to 3.1N HCl, and U and Pb were separated on anion-exchange columns².

Isotopic analyses were carried out on a VG sector 54 TIMS at MIT. U and Pb were loaded in silica gel³ onto out-gassed zone-refined Re filaments. Pb isotopes were measured by peak-hopping on the Daly detector and fractionation corrected based on repeat analyses of NBS 981, using the isotopic composition of Baker et al.⁴. U isotopes were measured statically on Faraday cups and fractionation-corrected using the ²³³U-²³⁵U double spike. All data reduction, error propagation and plotting of U-Pb data was done using the U-Pb_Redux software package^{5,6}.

The data were corrected for laboratory blank based on the isotopic composition of repeat analyses of total procedural blanks. Our experience based on thousands of chemical abrasion zircon analyses is that zircons do not typically include measurable common Pb (Pb_c) in their crystal structure. Microbeam analyses (e.g. secondary ion mass spectrometry and laser ablation) and TIMS analyses of untreated grains often record variable concentrations of Pb_c, however, the excess Pb_c may be derived from surface contamination, cracks or micro-inclusions. The initial digestion step in the chemical abrasion analyses cleans the grains and dissolves inclusions and damaged parts of the zircon structure. In almost all chemical abrasion analyses, including the analyses for this study, the total Pb_c in the final digestion step is indistinguishable from total procedural Pb blanks. We therefore assume that all ²⁰⁴Pb in the analyzed grains is derived from procedural blanks.

Total Pb_c ranged from 0.17–0.70 pg with Pb*/Pb_c = 0.18–3.42 (Supplementary Table S2; Pb*, radiogenic Pb). We analyzed 19 total procedural blanks for isotopic composition during this study, which spanned 1.5 years. Three blanks were excluded due to anomalous isotopic

compositions, which are most likely artifacts of isobaric interferences. The remaining 16 analyses had total Pb = 0.242–0.897 pg and mean isotopic compositions of $^{206}\text{Pb}/^{204}\text{Pb} = 18.638 \pm 0.707$, $^{207}\text{Pb}/^{204}\text{Pb} = 15.494 \pm 0.449$ and $^{208}\text{Pb}/^{204}\text{Pb} = 37.748 \pm 1.227$: reported uncertainties are $\pm 2\xi$ estimates of the overdispersion of the data, in excess of the analytical uncertainties, calculated following Vermeesch⁷. Analytical uncertainties, reported as 2σ confidence intervals, are generally dominated by variability in the isotopic composition of the laboratory blank, due to the low total Pb* in the analyzed grains.

An important consideration in U-Pb geochronology of ~1 Ma samples is how to accurately correct for initial secular disequilibrium in the U-Pb decay chains. ^{238}U and ^{235}U decay to ^{206}Pb and ^{207}Pb through a series of intermediate daughter products generated by alpha and beta decays. During zircon crystallization, the intermediate daughter products can be preferentially incorporated into or excluded from the crystal, relative to their parent U isotopes, depending on the zircon/magma distribution coefficient (D) for each element. A primary concern for the ^{238}U decay chain is exclusion of ^{230}Th , a long-lived intermediate daughter product ($t_{1/2} = 75,380$ years)⁸. An initial depletion in ^{230}Th leads to a deficiency in ^{206}Pb and erroneously young apparent $^{206}\text{Pb}/^{238}\text{U}$ dates. This effect is routinely corrected for using the Th/U of the zircon, which is typically a model Th/U calculated from the measured $^{208}\text{Pb}/^{206}\text{Pb}$ of the zircon, and an estimated Th/U of the magma. The maximum correction assuming complete Th exclusion is ~0.110 Ma and the uncertainties associated with the correction can be a major source of uncertainty in the absolute age of young zircons.

Model Th/U in the analyzed EPR zircons range from 0.33–2.77 (Supplementary Table S2). We applied two end-member approaches for Th-correcting the zircon data, using i) a constant Th/U of the magma, and ii) a constant zircon/magma $D_{\text{Th/U}}$ ($D_{\text{Th/U}} = D_{\text{Th}}/D_{\text{U}}$; Supplementary Figure S3, Supplementary Table S2). The former approach is the standard method for Th-correcting U-Pb dates and we present these results in the manuscript (Supplementary Figure S1a). For this correction, we used the mean and standard deviation of the Th/U of erupted EPR lavas as an estimate of the mean and variability of the Th/U of the magma. It is necessary to account for both the total Th/U of EPR glasses and the potential for excess ^{230}Th in mid-ocean ridge (MOR) magmas. Recently erupted mid-ocean ridge basalts (MORB) commonly have $(^{230}\text{Th})/(^{238}\text{U}) > 1$ (parentheses denote activities), which are interpreted to reflect differences in the Th and U crystal/liquid distribution coefficients during deep (>1.5 GPa) mantle melting (e.g.,⁹). Excess ^{230}Th in the magma reduces the magnitude of initial secular disequilibrium in crystallizing zircons and can be treated as a decrease in the effective Th/U of the magma (Appendix A of McLean et al.⁶).

Isotope dilution measurements on basaltic glasses from the EPR have Th/U = 1.68–3.33 (all but one data point have Th/U ≥ 2.25) with a mean of 2.51 ± 0.33 and $(^{230}\text{Th})/(^{238}\text{U}) = 1–1.233$ with a mean of 1.124 ± 0.093 ⁹⁻¹⁷ (n = 75; 2σ standard deviations). Dividing the mean Th/U by the mean $(^{230}\text{Th})/(^{238}\text{U})$ of the EPR glasses yields an effective Th/U of the lavas of 2.23 ± 0.31 (n = 75; uncertainty calculated using standard error propagation and includes covariance), which we interpret as the best estimate of the effective Th/U of mafic EPR magmas.

Application of the constant magma Th/U model implies that the observed variation in the Th/U of the dated zircons must reflect variations in the zircon/magma Th/U distribution coefficient ($D_{\text{Th/U}}$). Limited experiments on Th and U partitioning between zircon and melt record $D_{\text{Th/U}} = 0.25–0.95$ ^{18,19} ($f\text{O}_2 \sim \text{NNO}$, n = 13) and show a weak correlation with temperature. For a constant effective magma Th/U = 2.23, the observed Th/U in the EPR zircons require $D_{\text{Th/U}} = 0.15–1.24$. The majority of the predicted $D_{\text{Th/U}}$ are consistent with the experimental values, but

two high Th/U zircons from JC21-78R-1 require $D_{\text{Th/U}} > 1$, implying inclusion of excess Th. The scarcity of reversely discordant zircons suggests that $D_{\text{Th/U}}$ is typically less than 1 and we consider it unlikely that there was excess ^{230}Th included in the two high Th/U grains. The high Th/U may instead reflect variations in the Th/U of the magma.

For the second end-member correction, we assumed a constant $D_{\text{Th/U}}$ and a varying Th/U of the magma. We experimented with a range of $D_{\text{Th/U}}$ values, within the range of observed experimental values, and report results for $D_{\text{Th/U}} = 0.25$ and 0.85 (Supplementary Table S2, Supplementary Figure S3b, c; at temperatures below 1100°C the experimental $D_{\text{Th/U}} = 0.25$ to $0.82^{18,19}$). The predicted Th/U of the magmas, calculated from the observed Th/U of the zircon and the assumed $D_{\text{Th/U}}$, are 1.3–11.1 ($D_{\text{Th/U}} = 0.25$) and 0.4–3.3 ($D_{\text{Th/U}} = 0.85$). The calculated range in magmatic composition is significantly larger than the range of compositions observed in EPR glasses, which is discussed in detail below. Simultaneous decay of excess ^{230}Th during protracted zircon crystallization could also lead to an increase in the effective Th/U of the magma through time, although this effect would be small compared to the variations predicted by the constant $D_{\text{Th/U}}$ models.

The difference between the constant magma Th/U correction and the constant $D_{\text{Th/U}}$ corrections is dependent on the Th/U of the zircon (Supplementary Table S2, Supplementary Figure S3). The constant magma Th/U approach leads to variable Th-corrections for each grain (-0.026 to $+0.093$ Ma), with the magnitude of the correction being proportional to the difference between the effective Th/U of the magma and the Th/U of the zircon. The constant $D_{\text{Th/U}}$ model leads to a constant Th-correction for each grain, with Th-corrections of $+0.082$ Ma for $D_{\text{Th/U}} = 0.25$ and $+0.016$ Ma for $D_{\text{Th/U}} = 0.85$. The data corrected with a constant $D_{\text{Th/U}}$ have greater variability than the constant magma Th/U data, reflecting the original variability in the uncorrected dates.

The two end-member Th-correction models simplify complex systems and the variations in Th/U in the Hess Deep zircons may reflect a combination of changes in the Th/U of the magma and the zircon/magma distribution coefficients. The variability in the $^{206}\text{Pb}/^{238}\text{U}$ dates within each sample could, in principal, be explained by initial ^{230}Th disequilibrium if the difference between the Th/U of the magma and the Th/U of the zircon is minimized for the grains with the oldest uncorrected dates and maximized for the grains with the youngest uncorrected dates. To minimize the Th-correction for the grains with the oldest uncorrected dates in sample JC21-78R-5, the Th/U of the magma would have to be significantly lower (effective Th/U < 1.6) than the Th/U of EPR glasses (effective Th/U = 2.23). However, both theoretical predictions and natural data suggest that this is unlikely, because crystallization does not significantly affect Th/U. First, a study of a suite of EPR glasses that range from basaltic to andesitic compositions, the latter of which is expected to crystallize zircon, record Th/U of ~ 2.5 (effective Th/U ~ 2.2) over the full range in Mg# ($0.27\text{--}0.63$)²⁰, consistent with the average isotope dilution Th/U of basaltic EPR glasses. Second, because Th and U partition coefficients are both low and similar in an assemblage of olivine, plagioclase and pyroxene, fractionation modeling indicates that fractional crystallization in lower crustal magma chambers will not change Th/U by more than 3% over 90% crystallization. Apatite and zircon crystallization are also expected to have a limited impact on the Th/U of the melt. Experiments on trace element partitioning between apatite and a range of silicate melt compositions measured D_{U} and D_{Th} near unity²¹, consistent with observations from natural samples²². Further, data from natural samples suggest that apatite does not fractionate Th from U²². Apatite crystallization is therefore not expected to have a significant impact on the Th/U of the melt. Zircon has higher D_{Th} and D_{U} ^{18,19,22}

and Th/U that are generally lower than the effective Th/U of basaltic EPR glasses, and zircon crystallization would therefore increase the Th/U of the melt. However, the generally low U concentrations of MOR zircon and the low total volume of zircon in oceanic gabbros makes it unlikely that zircon crystallization leads to high Th/U magmas. Taken together, all lines of evidence suggest that the Th/U of the melt is likely to either remain constant or increase during crystallization. Thus it is highly unlikely that melt Th/U was significantly less than the effective Th/U of EPR basalts.

For JC21-78R-5, using a minimum effective Th/U equal to the effective Th/U of measured EPR glasses (Th/U = 2.23) for the five grains with the oldest uncorrected dates and a highly elevated Th/U = 15 for all other grains, still results in an MSWD = 2.4 and calculated overdispersion parameter of 0.075 ± 0.13 Ma. For JC21-78R-1, it is theoretically possible to attribute the total variability in the $^{206}\text{Pb}/^{238}\text{U}$ dates to crystallization from variable magma compositions with effective Th/U > 2.23. Such scenarios require a minimum of two different magma compositions with different Th/U and variable $D_{\text{Th/U}}$ in each magma: e.g., Th/U = 3.0 and 6.0 with $D_{\text{Th/U}} = 0.22\text{--}0.90$ and $0.10\text{--}0.20$, respectively. However, the data discussed above suggest that crystallization is unlikely to generate such a large range in the Th/U of MOR magmas. We therefore conclude that differences in Th/U are unlikely to be of sufficient magnitude to explain the observed variability in dates in either sample.

The uncertainty associated with the Th-correction is dependent on the difference between the zircon Th/U and assumed magma Th/U⁶: large differences between the zircon and magma Th/U lead to near maximum corrections and minimize the uncertainty in the correction, whereas similar zircon and magma Th/U lead to smaller corrections and larger uncertainties in the correction. The constant magma Th/U and $D_{\text{Th/U}} = 0.25$ models predict large differences between the magma and zircon Th/U, which minimizes the propagated uncertainty from the correction. The $D_{\text{Th/U}} = 0.85$ model predicts similar zircon and magma Th/U, which increases the propagated uncertainties. The uncertainties from the Th-correction dominate the total uncertainties for the $D_{\text{Th/U}} = 0.85$ dates.

For samples where the isotopic composition of the blank is the largest source of uncertainty, the Th-corrected dates can have smaller uncertainties than the uncorrected dates. The reduced uncertainties are due to statistical correlation between the $^{206}\text{Pb}/^{204}\text{Pb}$ and $^{208}\text{Pb}/^{204}\text{Pb}$ of measured laboratory blanks ($\rho = 0.329$). For the Th-corrected $^{206}\text{Pb}/^{238}\text{U}$ age, correlated variations in the $^{208}\text{Pb}/^{204}\text{Pb}$ and $^{206}\text{Pb}/^{204}\text{Pb}$ of the blank have opposing effects. For example, a $^{208}\text{Pb}/^{204}\text{Pb}$ of the blank that is higher than the assumed blank $^{208}\text{Pb}/^{204}\text{Pb}$ increases the Th-corrected $^{206}\text{Pb}/^{238}\text{U}$ date, while a $^{206}\text{Pb}/^{204}\text{Pb}$ of the blank that is higher than the assumed blank $^{206}\text{Pb}/^{204}\text{Pb}$ decreases the Th-corrected $^{206}\text{Pb}/^{238}\text{U}$ date. As a result, the positive correlation between the $^{208}\text{Pb}/^{204}\text{Pb}$ and $^{206}\text{Pb}/^{204}\text{Pb}$ of the laboratory blanks decreases the uncertainty in the Th-corrected $^{206}\text{Pb}/^{238}\text{U}$ dates.

In addition to the new Hess Deep analyses, we also present re-reduced U-Pb data from the Vema lithospheric section²³ (11°N, MAR). The data reported in Supplementary Table S3 and plotted in Supplementary Figure S4 include both data from our original study of the Vema lithospheric section²³ and a limited number of new analyses for samples DR10-005 and VE2-5. All of the data have been re-reduced using the new U-Pb_Redux algorithms⁶ and the revised laboratory blank compositions based on the total procedural blanks measured during the EPR study. The revised blank compositions are based on a slightly larger data set of higher quality analyses, and we feel they provide a better estimate of the true isotopic composition and variability of the laboratory blanks. The new blank composition has larger uncertainties than the

original blank values used, due to increased scatter within the dataset, which increases the uncertainties of the Vema U-Pb dates. The data are Th-corrected using a constant magma Th/U estimated from the Th/U of basaltic glasses from 11–30°N on the Mid-Atlantic Ridge ($\text{Th}/\text{U}_{\text{MAR}} = 2.36 \pm 0.30$; $n = 10$)²⁴⁻²⁶, and the new reduction propagates the uncertainties on the Th/U of the magma. We only present a single Th-correction model for these data because the dated grains are older than the Hess Deep zircons and have more uniform Th/U, which makes the final dates significantly less sensitive to the Th-correction. We excluded six analyses with anomalously high total Pb (>1 pg) from the discussion of the data, the weighted mean MSWD and overdispersion calculations, and Supplementary Figure S4, because the mean value and variability of the blank isotopic composition may be different at high blank values (Lissenberg et al.²³). We feel that Supplementary Table S3 is a more accurate representation of the Vema dates and uncertainties and should be used in place of the original data table from Lissenberg et al.²³. The revisions to the dates and uncertainties do not significantly change our original interpretations and conclusions.

Supplementary Discussion—Spreading rate

To calculate a time-averaged Pacific-Cocos spreading rate from the new U-Pb zircon dates, it is necessary to account for the overlapping spreading centers at ~2°N on the EPR, southwest of Hess Deep (Figure 1). Lonsdale^{27,28} demonstrated that the eastern axis of the overlapping spreading centers is propagating southward at a rate of ~166 km/Ma (recalculated using the Pacific-Cocos spreading rate of DeMets et al.²⁹). The tectonic evolution of the Galapagos microplate region is extremely complicated and the pre-1.0 Ma history is poorly constrained, however, the axial discontinuity is thought to have been present prior to this time (e.g.,^{27,30}). Reconstruction of the axis geometry at ~1.3 Ma suggests that the dated samples were formed along the western spreading axis, prior to the southward propagation of the discontinuity. The half-spreading rate calculated using our U-Pb zircon dates and the distance to the northward projection of the modern western axis is ~68–70 km/Ma, in agreement with the spreading rate calculated from sea-floor magnetic anomalies of ~66.5 km/Ma²⁹ (best fit model); the minor offset between the two rates likely reflects uncertainty in the location of the western ridge axis at ~1.3 Ma.

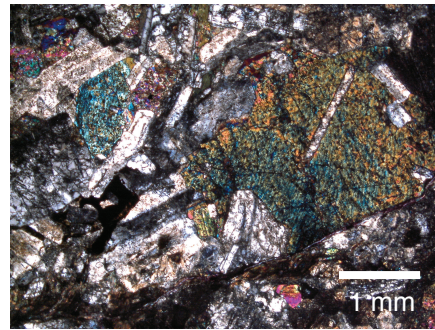
Supplementary References

- 1 Mattinson, J. M. Zircon U/Pb chemical abrasion (CA-TIMS) method; combined annealing and multi-step partial dissolution analysis for improved precision and accuracy of zircon ages. *Chem. Geol.* **220**, 47-66 (2005).
- 2 Krogh, T. E. Low-contamination method for hydrothermal decomposition of zircon and extraction of U and Pb for isotopic age determinations *Geochim. Cosmochim. Acta* **37**, 485-494 (1973).
- 3 Gerstenberger, H. & Haase, G. A highly effective emitter substance for mass spectrometric Pb isotope ratio determinations. *Chem. Geol.* **136**, 309-312 (1997).
- 4 Baker, J., Peate, D., Waight, T. & Meyzen, C. Pb isotopic analysis of standards and samples using a ²⁰⁷Pb-²⁰⁴Pb double spike and thallium to correct for mass bias with a double-focusing MC-ICP-MS. *Chem. Geol.* **211**, 275-303 (2004).
- 5 Bowring, J. F., McLean, N. M. & Bowring, S. A. Engineering cyber infrastructure for U-Pb geochronology: Tripoli and U-Pb_Redux. *Geochem., Geophys., Geosyst.* **12**, Q0AA19 (2011).

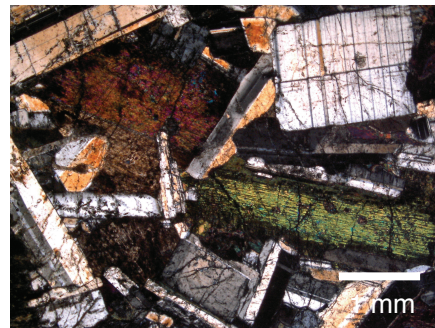
- 6 McLean, N. M., Bowring, J. F. & Bowring, S. A. An algorithm for U-Pb isotope dilution data reduction and uncertainty propagation. *Geochem. Geophys. Geosyst.* **12**, Q0AA18 (2011).
- 7 Vermeesch, P. HelioPlot, and the treatment of overdispersed (U-Th-Sm)/He data. *Chem. Geol.* **271**, 108-111 (2010).
- 8 Mattinson, J. M. Anomalous isotopic composition of lead in young zircons. *Carnegie Institution of Washington Yearbook* **72**, 613-616 (1973).
- 9 Sims, K. W. W. *et al.* Chemical and isotopic constraints on the generation and transport of magma beneath the East Pacific Rise. *Geochim. Cosmochim. Acta* **66**, 3481-3504 (2002).
- 10 Ben Othman, D. & Allègre, C. J. U-Th isotopic systematics at 13°N east Pacific Ridge segment. *Earth and Planet. Sci. Let.* **98**, 129-137 (1990).
- 11 Bourdon, B., Goldstein, S. J., Bourles, D., Murrell, M. T. & Langmuir, C. H. Evidence from ¹⁰Be and U series disequilibria on the possible contamination of mid-ocean ridge basalt glasses by sedimentary material. *Geochem. Geophys. Geosyst.* **1**, 1029 (2000).
- 12 Goldstein, S. J., Murrell, M. T. & Williams, R. W. ²³¹Pa and ²³⁰Th chronology of mid-ocean ridge basalts. *Earth and Planet. Sci. Let.* **115**, 151-159 (1993).
- 13 Lundstrom, C. C., Sampson, D. E., Perfit, M. R., Gill, J. & Williams, Q. Insights into mid-ocean ridge basalt petrogenesis: U-series disequilibria from the Siqueiros Transform, Lamont Seamounts, and East Pacific Rise. *J. Geophys. Res.* **104**, 13035-13048 (1999).
- 14 Rubin, K. H., van der Zander, I., Smith, M. C. & Bergmanis, E. C. Minimum speed limit for ocean ridge magmatism from ²¹⁰Pb-²²⁶Ra-²³⁰Th disequilibria. *Nature* **437**, 534-538 (2005).
- 15 Sims, K. W. W. *et al.* Aberrant youth: Chemical and isotopic constraints on the origin of off-axis lavas from the East Pacific Rise, 9°–10°N. *Geochem. Geophys. Geosyst.* **4**, 8621 (2003).
- 16 Volpe, A. M. & Goldstein, S. J. ²²⁶Ra-²³⁰Th disequilibrium in axial and off-axis mid-ocean ridge basalts. *Geochim. Cosmochim. Acta* **57**, 1233-1241 (1993).
- 17 Zou, H., Zindler, A. & Niu, Y. Constraints on Melt Movement Beneath the East Pacific Rise From ²³⁰Th-²³⁸U Disequilibrium. *Science* **295**, 107-110 (2002).
- 18 Luo, Y. & Ayers, J. C. Experimental measurements of zircon/melt trace-element partition coefficients. *Geochim. Cosmochim. Acta* **73**, 3656-3679 (2009).
- 19 Rubatto, D. & Hermann, J. Experimental zircon/melt and zircon/garnet trace element partitioning and implications for the geochronology of crustal rocks. *Chem. Geol.* **241**, 38-61 (2007).
- 20 Regelous, M. *et al.* Variations in the geochemistry of magmatism on the East Pacific Rise at 10°30'N since 800 ka. *Earth and Planet. Sci. Let.* **168**, 45-63, doi:10.1016/s0012-821x(99)00048-5 (1999).
- 21 Prowatke, S. & Klemme, S. Trace element partitioning between apatite and silicate melts. *Geochim. Cosmochim. Acta* **70**, 4513-4527, doi:10.1016/j.gca.2006.06.162 (2006).
- 22 Farley, K. A., Kohn, B. P. & Pillans, B. The effects of secular disequilibrium on (U-Th)/He systematics and dating of Quaternary volcanic zircon and apatite. *Earth and Planet. Sci. Let.* **201**, 117-125, doi:10.1016/s0012-821x(02)00659-3 (2002).
- 23 Lissenberg, C. J., Rioux, M., Shimizu, N., Bowring, S. A. & Mevel, C. Zircon dating of oceanic crustal accretion. *Science* **323**, 1048-1050, doi:10.1126/science.1167330 (2009).

- 24 Bourdon, B., Zindler, A., Elliott, T. & Langmuir, C. H. Constraints on mantle melting at mid-ocean ridges from global ^{238}U - ^{230}Th disequilibrium data. *Nature* **384**, 231-235 (1996).
- 25 Sturm, M. E., Goldstein, S. J., Klein, E. M., Karson, J. A. & Murrell, M. T. Uranium-series age constraints on lavas from the axial valley of the Mid-Atlantic Ridge, MARK area. *Earth and Planet. Sci. Let.* **181**, 61-70 (2000).
- 26 White, W. M. $^{238}\text{U}/^{204}\text{Pb}$ in MORB and open system evolution of the depleted mantle. *Earth and Planet. Sci. Let.* **115**, 211-226 (1993).
- 27 Lonsdale, P. The rise flank trails left by migrating offsets of the equatorial East Pacific Rise axis. *J. Geophys. Res.* **94**, 713-743 (1989).
- 28 Lonsdale, P. Structural pattern of the Galapagos Microplate and evolution of the Galapagos Triple Junctions. *J. Geophys. Res.* **93**, 13551-13574 (1988).
- 29 DeMets, C., Gordon, R. G. & Argus, D. F. Geologically current plate motions. *Geophys. J. Int.* **181**, 1-80 (2010).
- 30 Schouten, H., Smith, D. K., Montési, L. G. J., Zhu, W. & Klein, E. M. Cracking of lithosphere north of the Galapagos triple junction. *Geology* **36**, 339-342 (2008).

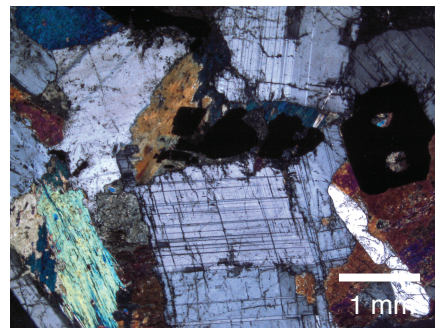
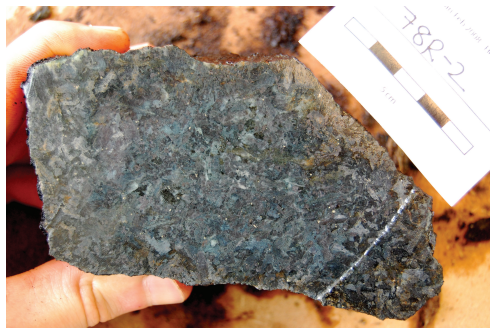
JC21-76R-4



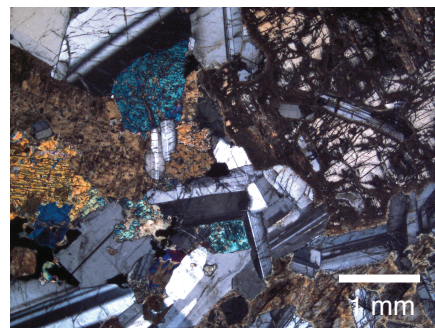
JC21-78R-1



JC21-78R-2

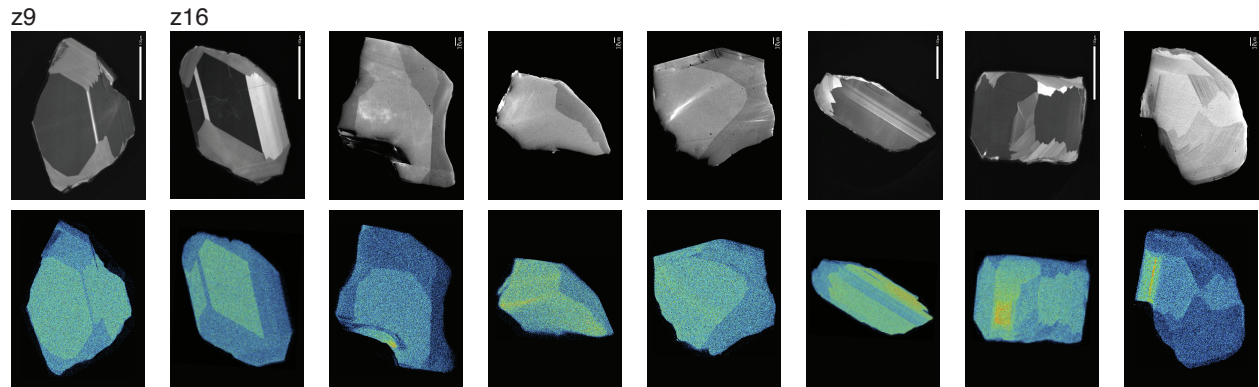


JC21-78R-5

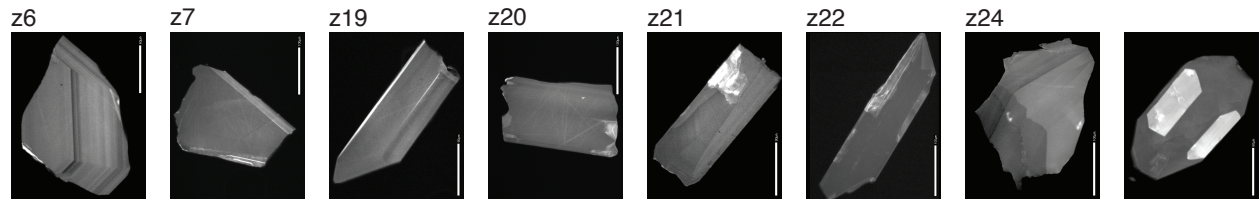


Supplementary Figure S1 Hand sample and thin section (cross-polarized) photos of each of the dated samples. The full scale bars in the hand sample photos are 5 cm.

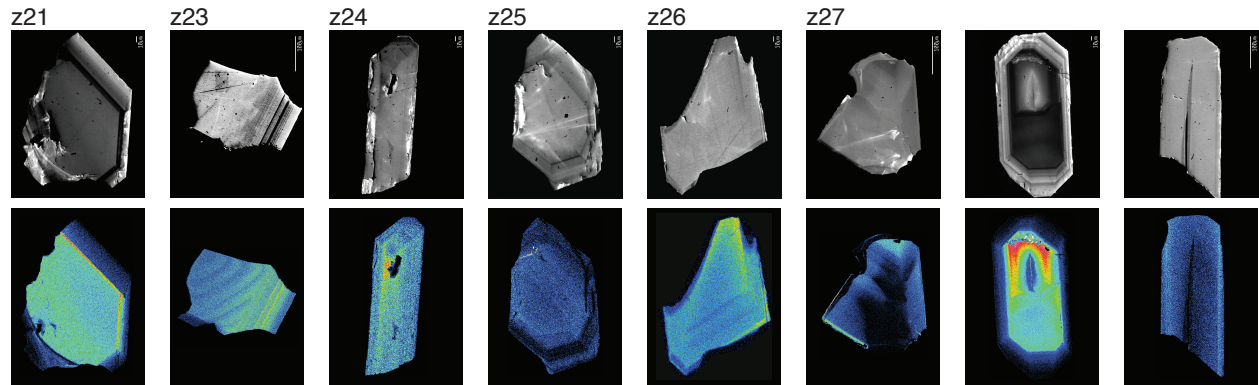
JC21-76R-4



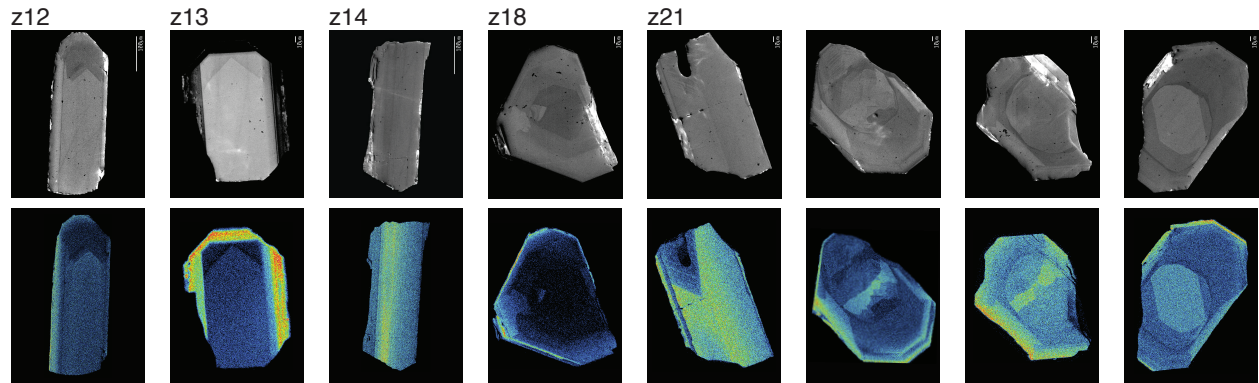
JC21-78R-1



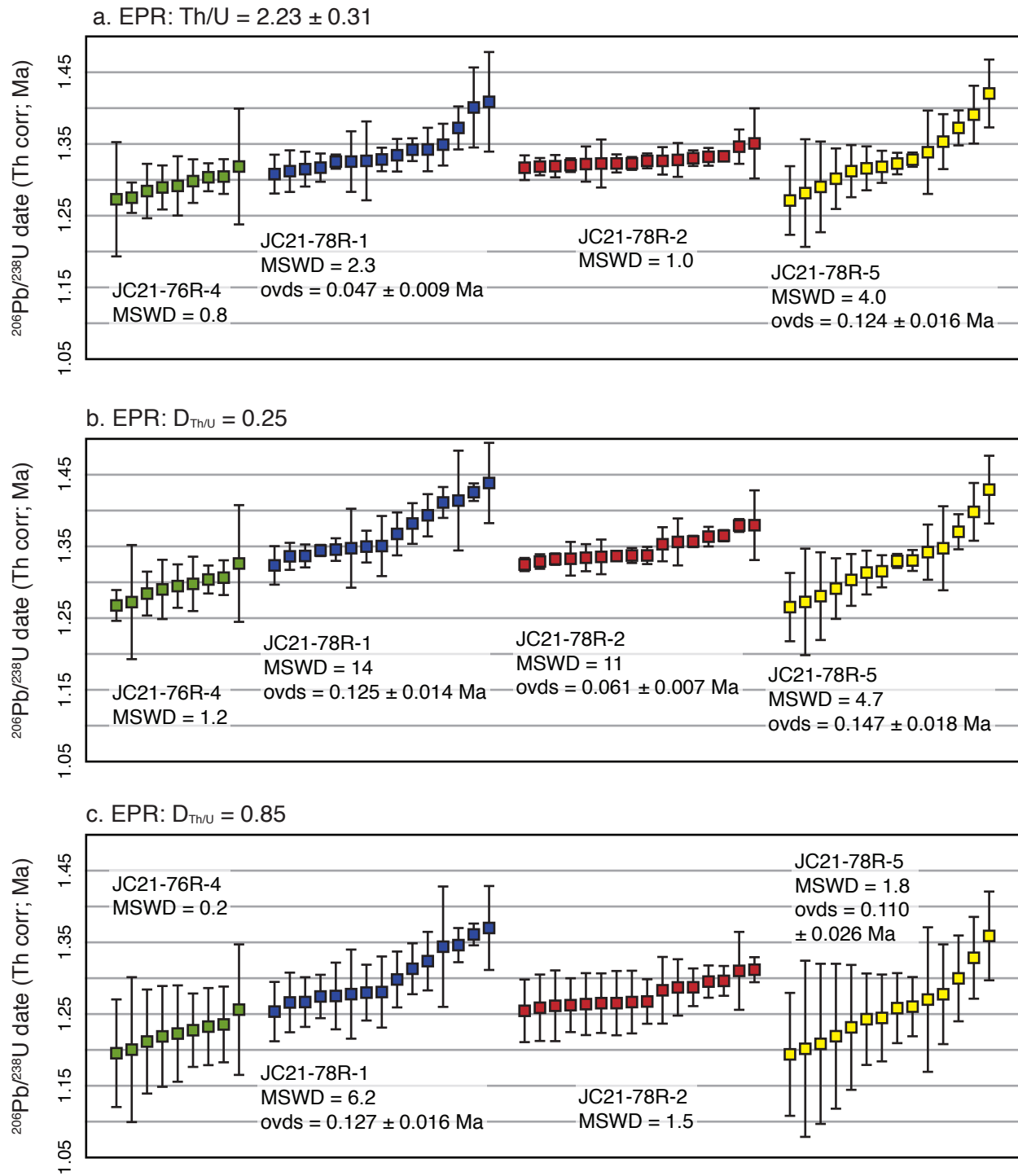
JC21-78R-2



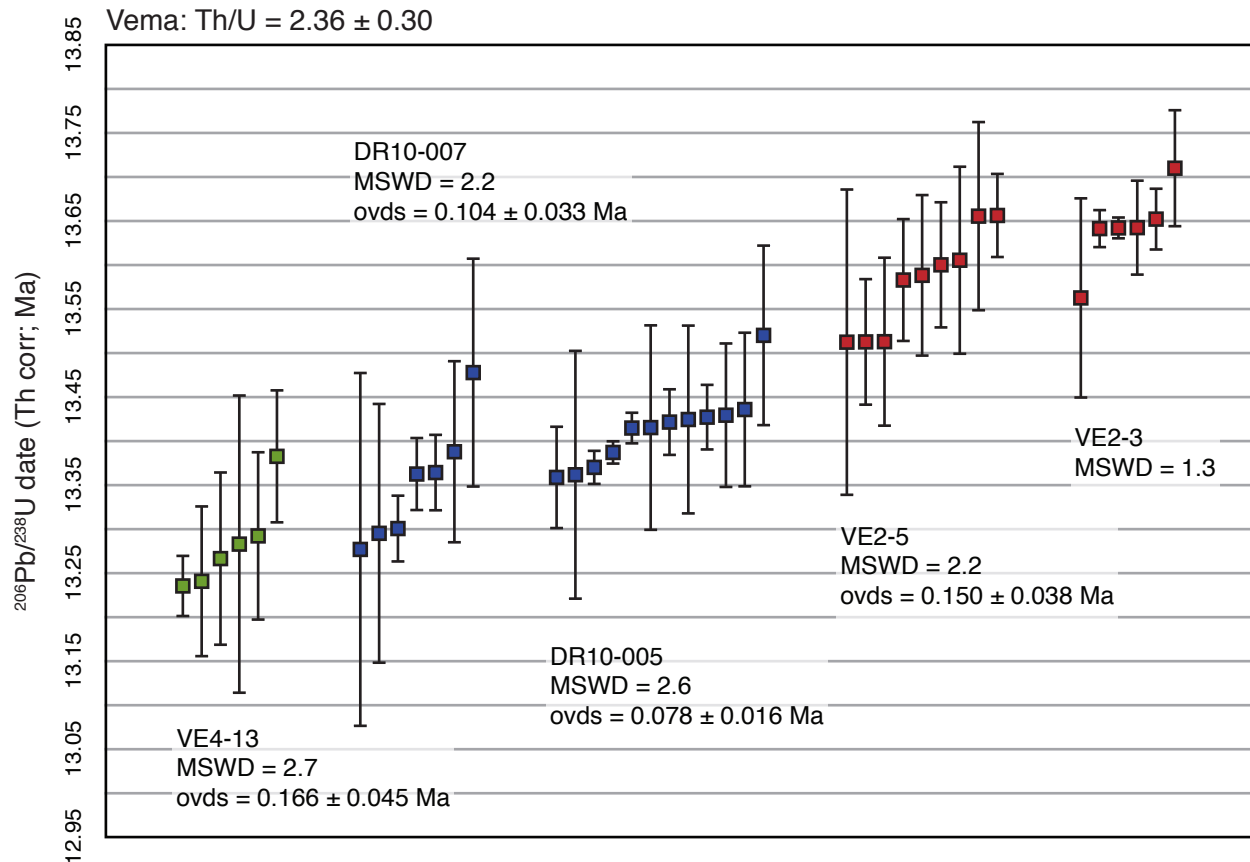
JC21-78R-5



Supplementary Figure S2 Cathodoluminescence images (gray scale) and Y maps (color) of representative grains from each sample. Numbered images (e.g., z1) correspond to dated grains in Supplementary Table 2.



Supplementary Figure S3 Single grain and grain fragment $^{206}\text{Pb}/^{238}\text{U}$ zircon dates from Hess Deep reduced using three different Th-corrections. Uncertainties are represented as 2σ confidence intervals. Overdispersion (ovds) in dates calculated following Vermeesch⁷.



Supplementary Figure S4 Single grain and grain fragment $^{206}\text{Pb}/^{238}\text{U}$ zircon dates from the Vema lithospheric section. Data are from Lissenberg et al.²⁵ and new analyses presented here (Supplementary Table 3). All of the data were re-reduced using the U-Pb_Redux algorithms⁶ and a revised blank isotopic composition, and are Th-corrected assuming a constant magma Th/U = 2.36 ± 0.30 (2σ). The data are plotted to the same scale as the Hess Deep analyses in Supplementary Figure 3. Uncertainties are represented as 2σ confidence intervals. Overdispersion (ovds) in dates calculated following Vermeesch⁷.

Supplementary Table S1 Sample locations

Sample	Latitude	Longitude	Depth (mbsl)
JC21-76R-4	2.293	101.533	3451
JC21-78R-1	2.308	101.522	3160
JC21-78R-2	2.308	101.523	3132
JC21-78R-5	2.308	101.523	3116

Supplementary Table S2 Single grain ID-TIMS U-Pb zircon data from Hess Deep

Composition				Isotopic Ratios									
Pb*/ ^a	Pb* ^b	Pbc ^b	Th/ ^c	Uncorrected									
Pbc	(pg)	(pg)	U	²⁰⁶ Pb/ ^d	²⁰⁸ Pb/ ^e	²⁰⁶ Pb*/ ^e	2σ	²⁰⁷ Pb*/ ^e	2σ	²⁰⁷ Pb*/ ^e	2σ	corr. ^f	
				²⁰⁴ Pb	²⁰⁶ Pb	²³⁸ U	(% err)	²³⁵ U	(% err)	²⁰⁶ Pb*	(% err)	coef.	
JC21-78R-1													
z1	1.07	0.25	0.24	0.723	79.0	0.24537	0.0001946	1.308	0.00145	15.91	0.05411	15.53	0.331
z2	2.51	0.62	0.25	0.935	152.8	0.31454	0.0001957	0.611	0.00137	7.87	0.05062	7.67	0.370
z4	2.75	0.72	0.26	2.768	123.2	0.86904	0.0002081	0.916	0.00150	12.38	0.05235	11.90	0.559
z6	1.26	0.28	0.22	2.537	68.4	0.80352	0.0002059	1.625	0.00131	24.06	0.04619	23.49	0.377
z7	0.39	0.09	0.22	1.307	37.6	0.43272	0.0002103	4.213	0.00218	40.70	0.07526	39.19	0.403
z8	1.21	0.30	0.25	0.627	88.6	0.21331	0.0001960	1.302	0.00149	16.18	0.05532	15.59	0.489
z10	0.74	0.18	0.25	1.214	55.4	0.40367	0.0002015	2.231	0.00189	22.05	0.06796	21.28	0.390
z14	0.42	0.17	0.41	1.058	40.8	0.35431	0.0001967	3.369	0.00124	49.32	0.04556	48.48	0.280
z15	0.63	0.25	0.39	1.060	51.6	0.35485	0.0001993	2.386	0.00148	30.50	0.05393	29.71	0.368
z17	0.76	0.32	0.42	0.866	60.1	0.29206	0.0001966	1.781	0.00143	22.37	0.05292	21.97	0.259
z19	0.24	0.09	0.40	0.661	32.3	0.22395	0.0002066	5.387	0.00155	65.76	0.05450	64.60	0.254
z20	0.61	0.29	0.47	0.978	51.0	0.32813	0.0002034	2.282	0.00167	24.89	0.05964	24.42	0.249
z21	0.91	0.39	0.43	0.940	67.6	0.31619	0.0001945	1.528	0.00118	23.78	0.04406	23.41	0.277
z22	0.32	0.13	0.41	0.978	35.6	0.32848	0.0001962	4.447	0.00107	76.66	0.03937	75.43	0.305
z24	0.65	0.30	0.47	0.867	54.2	0.29261	0.0001925	2.232	0.00107	36.59	0.04022	35.86	0.353
JC21-78R-2													
z4	2.34	1.20	0.51	0.744	150.0	0.25225	0.0001939	0.613	0.00140	7.66	0.05239	7.46	0.354
z9	3.42	0.93	0.27	0.633	216.2	0.21534	0.0001946	0.392	0.00142	4.70	0.05274	4.61	0.259
z10	2.17	0.59	0.27	0.643	144.1	0.21891	0.0001928	0.740	0.00124	10.43	0.04675	10.08	0.500
z11	0.89	0.24	0.26	0.713	69.1	0.24203	0.0001942	1.552	0.00142	19.60	0.05308	19.13	0.335
z12	1.78	0.52	0.29	0.934	114.4	0.31439	0.0001947	0.834	0.00126	11.61	0.04678	11.36	0.339
z13	1.59	0.58	0.36	1.489	94.1	0.49062	0.0001987	1.078	0.00148	13.10	0.05414	12.74	0.366
z16	2.35	0.96	0.41	1.091	139.4	0.36468	0.0001977	0.608	0.00150	7.04	0.05492	6.93	0.224
z17	0.69	0.27	0.40	0.693	57.7	0.23519	0.0001971	1.918	0.00156	22.08	0.05747	21.62	0.277
z18	2.45	1.29	0.53	1.757	128.9	0.57286	0.0002010	0.689	0.00136	9.50	0.04889	9.33	0.290
z20	0.69	0.29	0.42	0.825	56.7	0.27868	0.0001944	1.968	0.00119	29.15	0.04428	28.68	0.268
z21	2.53	1.44	0.57	1.397	141.2	0.46165	0.0001989	0.605	0.00135	8.00	0.04908	7.87	0.250
z23	0.69	0.48	0.70	0.658	57.9	0.22389	0.0001940	1.932	0.00139	24.76	0.05199	24.26	0.294
z24	0.39	0.17	0.45	1.132	38.3	0.37770	0.0002012	3.811	0.00187	37.14	0.06759	36.25	0.282
z25	0.59	0.25	0.43	1.226	48.2	0.40781	0.0001976	2.616	0.00125	38.58	0.04583	37.77	0.339
z26	1.38	0.57	0.41	0.663	97.6	0.22554	0.0001947	0.950	0.00136	12.34	0.05083	12.13	0.261
z27	1.67	0.73	0.44	0.608	116.2	0.20723	0.0001934	0.792	0.00132	10.13	0.04962	9.93	0.294

Supplementary Table S2 Continued

	Isotopic Ratios														
	Th-corrected (Th/U = 2.23 ± 0.31)					Th-corrected ($D_{Th/U} = 0.25$)					Th-corrected ($D_{Th/U} = 0.85$)				
	$^{206}Pb^*/^c$	2σ	$^{207}Pb^*/^c$	2σ	corr. ^f	$^{206}Pb^*/^c$	2σ	$^{207}Pb^*/^c$	2σ	corr. ^f	$^{206}Pb^*/^c$	2σ	$^{207}Pb^*/^c$	2σ	corr. ^f
^{238}U	(% err)	$^{206}Pb^*$	(% err)	coef.	^{238}U	(% err)	$^{206}Pb^*$	(% err)	coef.	^{238}U	(% err)	$^{206}Pb^*$	(% err)	coef.	
JC21-78R-1															
z1	0.0002061	1.234	0.05109	15.66	0.239	0.0002074	1.197	0.05078	15.63	0.268	0.0001964	3.286	0.05361	16.16	0.025
z2	0.0002056	0.746	0.04819	7.74	0.221	0.0002086	0.582	0.04751	7.71	0.315	0.0001977	2.375	0.05011	8.12	0.046
z4	0.0002040	1.845	0.05340	12.07	0.242	0.0002212	0.859	0.04926	11.94	0.546	0.0002111	1.117	0.05160	11.97	0.409
z6	0.0002036	2.210	0.04672	23.67	0.219	0.0002190	1.527	0.04343	23.55	0.361	0.0002088	1.773	0.04554	23.61	0.288
z7	0.0002173	3.984	0.07282	39.62	0.315	0.0002232	3.894	0.07092	39.42	0.372	0.0002125	4.274	0.07446	39.83	0.253
z8	0.0002082	1.182	0.05207	15.76	0.392	0.0002088	1.170	0.05193	15.74	0.409	0.0001978	3.647	0.05480	16.44	0.042
z10	0.0002093	2.160	0.06545	21.51	0.297	0.0002144	2.054	0.06389	21.40	0.357	0.0002037	2.705	0.06724	21.68	0.196
z14	0.0002056	3.187	0.04358	48.78	0.199	0.0002095	3.106	0.04277	48.66	0.242	0.0001987	3.872	0.04510	49.07	0.103
z15	0.0002082	2.260	0.05162	29.96	0.276	0.0002121	2.188	0.05067	29.86	0.327	0.0002014	3.002	0.05337	30.21	0.147
z17	0.0002070	1.704	0.05026	22.13	0.178	0.0002094	1.643	0.04968	22.07	0.212	0.0001986	3.041	0.05240	22.45	0.040
z19	0.0002186	4.930	0.05152	65.02	0.186	0.0002194	4.922	0.05133	64.96	0.198	0.0002085	6.249	0.05401	65.93	0.019
z20	0.0002129	2.184	0.05697	24.60	0.174	0.0002162	2.112	0.05611	24.53	0.211	0.0002054	3.083	0.05906	24.86	0.069
z21	0.0002043	1.496	0.04194	23.56	0.180	0.0002073	1.410	0.04134	23.50	0.227	0.0001965	2.735	0.04361	23.82	0.043
z22	0.0002058	4.145	0.03754	75.83	0.228	0.0002091	4.086	0.03696	75.68	0.265	0.0001982	4.862	0.03897	76.23	0.121
z24	0.0002029	2.070	0.03816	36.09	0.269	0.0002053	2.029	0.03771	36.02	0.306	0.0001945	3.304	0.03982	36.43	0.092
JC21-78R-2															
z4	0.0002052	0.678	0.04950	7.53	0.227	0.0002067	0.594	0.04915	7.51	0.280	0.0001958	2.975	0.05188	8.15	0.022
z9	0.0002068	0.484	0.04964	4.66	0.137	0.0002074	0.436	0.04950	4.65	0.160	0.0001963	3.544	0.05229	5.89	-0.001
z10	0.0002049	0.724	0.04399	10.19	0.368	0.0002055	0.692	0.04385	10.18	0.400	0.0001946	3.480	0.04630	10.92	0.025
z11	0.0002058	1.444	0.05010	19.29	0.248	0.0002070	1.415	0.04980	19.26	0.273	0.0001961	3.417	0.05258	19.78	0.032
z12	0.0002045	0.912	0.04452	11.44	0.224	0.0002075	0.780	0.04389	11.41	0.292	0.0001966	2.449	0.04631	11.74	0.054
z13	0.0002043	1.307	0.05264	12.86	0.226	0.0002116	1.004	0.05084	12.79	0.339	0.0002009	1.737	0.05352	12.94	0.157
z16	0.0002064	0.816	0.05261	6.99	0.112	0.0002105	0.582	0.05157	6.95	0.187	0.0001997	2.041	0.05436	7.27	0.029
z17	0.0002089	1.778	0.05425	21.79	0.201	0.0002099	1.756	0.05398	21.76	0.219	0.0001991	3.623	0.05692	22.30	0.019
z18	0.0002046	1.179	0.04803	9.44	0.117	0.0002140	0.649	0.04594	9.35	0.264	0.0002035	1.329	0.04829	9.46	0.100
z20	0.0002051	1.857	0.04197	28.86	0.190	0.0002072	1.809	0.04155	28.81	0.220	0.0001963	3.285	0.04385	29.20	0.041
z21	0.0002052	0.954	0.04756	7.95	0.110	0.0002118	0.574	0.04609	7.89	0.221	0.0002011	1.606	0.04854	8.07	0.056
z23	0.0002060	1.779	0.04896	24.44	0.214	0.0002068	1.762	0.04878	24.42	0.229	0.0001957	3.911	0.05153	25.03	0.011
z24	0.0002096	3.618	0.06489	36.57	0.205	0.0002140	3.524	0.06353	36.42	0.248	0.0002033	4.147	0.06690	36.84	0.129
z25	0.0002052	2.530	0.04412	38.03	0.248	0.0002104	2.415	0.04303	37.91	0.305	0.0001997	3.054	0.04534	38.20	0.163
z26	0.0002067	0.930	0.04789	12.21	0.174	0.0002075	0.896	0.04770	12.20	0.193	0.0001965	3.450	0.05037	12.81	0.002
z27	0.0002058	0.781	0.04664	10.00	0.205	0.0002062	0.761	0.04655	9.99	0.216	0.0001953	3.680	0.04914	10.76	0.005

Supplementary Table S2 Continued

Dates																		
Uncorrected				Th-corrected (Th/U = 2.23 ± 0.31)				Th-corrected (D _{Th/U} = 0.25)				Th-corrected (D _{Th/U} = 0.85)						
²⁰⁶ Pb/g	2σ	²⁰⁷ Pb/g	2σ	²⁰⁷ Pb/g	2σ	²⁰⁶ Pb/g	2σ	²⁰⁷ Pb/g	2σ	²⁰⁶ Pb/g	2σ	²⁰⁷ Pb/g	2σ	²⁰⁶ Pb/g	2σ	²⁰⁷ Pb/g	2σ	
²³⁸ U	(abs)	²³⁵ U	(abs)	²⁰⁶ Pb	(abs)	²³⁸ U	(abs)	²⁰⁶ Pb	(abs)	²³⁸ U	(abs)	²⁰⁶ Pb	(abs)	²³⁸ U	(abs)	²⁰⁶ Pb	(abs)	
JC21-78R-1																		
z1	1.254	0.016	1.47	0.23	376	349	1.328	0.016	245	361	1.337	0.016	231	361	1.266	0.042	355	365
z2	1.262	0.008	1.39	0.11	224	177	1.325	0.010	109	183	1.344	0.008	75	183	1.274	0.030	200	189
z4	1.341	0.012	1.52	0.19	301	271	1.315	0.024	346	273	1.426	0.012	160	279	1.361	0.015	268	275
z6	1.327	0.022	1.33	0.32	7	565	1.312	0.029	35	567	1.411	0.022	-143	583	1.346	0.024	-27	572
z7	1.356	0.057	2.21	0.90	1075	787	1.401	0.056	1009	804	1.438	0.056	955	806	1.370	0.059	1054	802
z8	1.263	0.016	1.52	0.25	425	348	1.342	0.016	288	360	1.346	0.016	282	360	1.275	0.047	404	368
z10	1.299	0.029	1.92	0.42	867	441	1.349	0.029	789	451	1.382	0.028	738	453	1.313	0.036	845	451
z14	1.268	0.043	1.25	0.62	-26	1174	1.325	0.042	-134	1207	1.351	0.042	-181	1215	1.281	0.050	-50	1194
z15	1.285	0.031	1.50	0.46	368	669	1.342	0.030	269	687	1.367	0.030	226	690	1.298	0.039	345	683
z17	1.267	0.023	1.46	0.33	325	499	1.334	0.023	207	513	1.350	0.022	180	514	1.280	0.039	303	512
z19	1.332	0.072	1.58	1.04	392	1449	1.409	0.069	264	1492	1.414	0.070	256	1493	1.344	0.084	371	1485
z20	1.311	0.030	1.70	0.42	591	529	1.372	0.030	490	543	1.393	0.029	457	544	1.324	0.041	569	541
z21	1.254	0.019	1.20	0.29	-107	576	1.317	0.020	-230	594	1.336	0.019	-267	597	1.267	0.035	-133	589
z22	1.265	0.056	1.08	0.83	-392	1964	1.326	0.055	-517	2026	1.348	0.055	-560	2040	1.278	0.062	-419	1996
z24	1.241	0.028	1.08	0.40	-337	923	1.308	0.027	-474	956	1.324	0.027	-506	960	1.253	0.041	-363	943
JC21-78R-2																		
z4	1.250	0.008	1.42	0.11	303	170	1.323	0.009	172	176	1.332	0.008	155	176	1.262	0.038	280	187
z9	1.254	0.005	1.44	0.07	318	105	1.333	0.006	178	109	1.337	0.006	171	109	1.265	0.045	298	134
z10	1.242	0.009	1.26	0.13	37	241	1.320	0.010	-111	251	1.325	0.009	-119	251	1.254	0.044	14	262
z11	1.252	0.019	1.44	0.28	332	434	1.326	0.019	199	448	1.334	0.019	186	448	1.264	0.043	311	450
z12	1.255	0.010	1.27	0.15	38	272	1.318	0.012	-82	280	1.337	0.010	-117	281	1.268	0.031	14	282
z13	1.280	0.014	1.50	0.20	377	287	1.317	0.017	313	293	1.364	0.014	233	295	1.295	0.022	351	292
z16	1.274	0.008	1.52	0.11	409	155	1.330	0.011	312	159	1.357	0.008	267	160	1.287	0.026	386	163
z17	1.271	0.024	1.59	0.35	510	475	1.346	0.024	381	490	1.353	0.024	370	490	1.283	0.046	488	492
z18	1.296	0.009	1.38	0.13	143	219	1.319	0.016	101	223	1.379	0.009	-6	226	1.312	0.017	114	223
z20	1.253	0.025	1.20	0.35	-95	704	1.322	0.025	-228	727	1.335	0.024	-254	729	1.265	0.042	-119	720
z21	1.282	0.008	1.37	0.11	152	184	1.323	0.013	78	189	1.365	0.008	3	190	1.296	0.021	126	190
z23	1.251	0.024	1.41	0.35	285	555	1.328	0.024	146	573	1.333	0.023	137	574	1.262	0.049	265	574
z24	1.297	0.049	1.90	0.71	856	753	1.351	0.049	771	770	1.380	0.049	726	772	1.310	0.054	835	768
z25	1.273	0.033	1.27	0.49	-11	912	1.323	0.033	-104	935	1.356	0.033	-166	944	1.287	0.039	-37	927
z26	1.255	0.012	1.38	0.17	233	280	1.332	0.012	94	289	1.337	0.012	85	289	1.267	0.044	212	297
z27	1.247	0.010	1.34	0.14	177	231	1.326	0.010	31	240	1.329	0.010	26	240	1.259	0.046	155	252

Supplementary Table S2 Continued

	Composition				Isotopic Ratios								
	Pb*/ ^a	Pb*/ ^b	Pbc ^b	Th/ ^c	Uncorrected								
					²⁰⁶ Pb/ ^d	²⁰⁸ Pb/ ^e	²⁰⁶ Pb*/ ^e	2σ	²⁰⁷ Pb*/ ^e	2σ	²⁰⁷ Pb*/ ^e	2σ	corr. ^f
Pbc	(pg)	(pg)	U	²⁰⁴ Pb	²⁰⁶ Pb	²³⁸ U	(% err)	²³⁵ U	(% err)	²⁰⁶ Pb*	(% err)	coef. ^f	
JC21-78R-5													
z1	1.77	0.64	0.36	0.590	121.7	0.20105	0.0001935	0.763	0.00144	9.20	0.05392	8.99	0.318
z2	0.52	0.23	0.43	0.508	49.8	0.17388	0.0001910	2.669	0.00134	37.01	0.05081	35.98	0.417
z3	0.71	0.35	0.50	0.499	61.0	0.17087	0.0001913	1.921	0.00147	23.22	0.05559	22.52	0.399
z5	0.30	0.12	0.42	0.442	36.9	0.15196	0.0001836	4.285	0.00089	81.17	0.03523	79.79	0.347
z6	0.23	0.07	0.28	0.367	33.5	0.12637	0.0001859	5.825	0.00056	198.49	0.02185	195.65	0.498
z7	0.36	0.24	0.68	0.732	38.9	0.24721	0.0002089	3.590	0.00178	37.59	0.06167	36.98	0.217
z8	0.40	0.14	0.36	0.384	43.8	0.13201	0.0001895	3.165	0.00072	77.98	0.02758	76.89	0.360
z10	0.32	0.12	0.37	0.349	38.9	0.12047	0.0001876	3.660	0.00125	50.90	0.04819	50.07	0.260
z11	0.37	0.23	0.62	0.332	41.7	0.11420	0.0001955	3.175	0.00132	42.31	0.04880	41.66	0.240
z12	0.66	0.17	0.26	0.517	58.3	0.17658	0.0001999	1.962	0.00124	27.89	0.04513	27.40	0.281
z13	1.17	0.31	0.26	0.711	84.9	0.24143	0.0001936	1.194	0.00125	17.40	0.04672	17.02	0.349
z14	0.18	0.06	0.30	0.380	30.2	0.13096	0.0001847	6.680	0.00050	229.06	0.01973	226.94	0.330
z18	0.42	0.16	0.39	0.701	42.1	0.23749	0.0002041	3.148	0.00193	30.61	0.06843	29.94	0.260
z21	0.29	0.13	0.44	0.735	34.8	0.24926	0.0001963	4.845	0.00161	58.82	0.05960	57.12	0.388
JC21-76R-4													
z1	0.52	0.18	0.34	0.487	49.9	0.16696	0.0001881	2.696	0.00117	40.78	0.04521	39.66	0.444
z2	0.65	0.17	0.26	0.410	59.1	0.14131	0.0001839	1.876	0.00102	31.51	0.04013	31.02	0.292
z4	0.68	0.17	0.25	0.595	58.6	0.20294	0.0001899	2.109	0.00127	30.62	0.04843	29.75	0.441
z5	0.86	0.16	0.18	0.562	69.5	0.19221	0.0001895	1.700	0.00127	25.08	0.04878	24.34	0.466
z6	0.49	0.08	0.17	0.455	48.6	0.15623	0.0001865	2.721	0.00120	40.79	0.04648	39.80	0.395
z7	0.43	0.18	0.42	0.824	42.1	0.27891	0.0001885	3.219	0.00131	43.13	0.05031	42.28	0.299
z8	0.36	0.12	0.34	0.526	40.0	0.18031	0.0001874	3.603	0.00140	44.08	0.05433	43.06	0.321
z9	0.19	0.06	0.34	0.548	29.8	0.18758	0.0001846	7.136	0.00134	92.36	0.05271	89.90	0.378
z16	0.20	0.09	0.42	0.711	30.1	0.24133	0.0001930	6.864	0.00162	78.37	0.06099	76.14	0.363

^a Ratio of radiogenic to common Pb.

^b Total radiogenic Pb and common Pb (picograms).

^c Th/U ratio calculated from ²⁰⁸Pb/²⁰⁶Pb and the ²⁰⁶Pb/²³⁸U date of the sample.

^d Fractionation and spike corrected isotopic ratios.

^e Fractionation, spike, and blank corrected radiogenic isotope ratios. Laboratory blanks were corrected using ²⁰⁶Pb/²⁰⁴Pb = 18.638 ± 0.707, ²⁰⁷Pb/²⁰⁴Pb = 15.494 ± 0.449, ²⁰⁸Pb/²⁰⁴Pb = 37.748 ± 1.227.

^f Correlation coefficient of radiogenic ²⁰⁷Pb/²³⁵U and ²⁰⁶Pb*/²³⁸U.

^g Dates (Ma) calculated using ²³⁸U/²³⁵U = 137.88, and decay constants of ²³⁸U = 1.5513 x 10⁻¹⁰ yr⁻¹ and ²³⁵U = 9.8485 x 10⁻¹⁰ yr⁻¹.

Supplementary Table S2 Continued

	Isotopic Ratios														
	Th-corrected (Th/U = 2.23 ± 0.31)					Th-corrected ($D_{Th/U} = 0.25$)					Th-corrected ($D_{Th/U} = 0.85$)				
	$^{206}Pb^{*/c}$	2σ	$^{207}Pb^{*/c}$	2σ	corr. ^f	$^{206}Pb^{*/c}$	2σ	$^{207}Pb^{*/c}$	2σ	corr. ^f	$^{206}Pb^{*/c}$	2σ	$^{207}Pb^{*/c}$	2σ	corr. ^f
^{238}U	(% err)	$^{206}Pb^{*}$	(% err)	coef.	^{238}U	(% err)	$^{206}Pb^{*}$	(% err)	coef.	^{238}U	(% err)	$^{206}Pb^{*}$	(% err)	coef.	
JC21-78R-5															
z1	0.0002060	0.748	0.05064	9.06	0.223	0.0002063	0.735	0.05058	9.06	0.232	0.0001952	3.881	0.05345	9.98	0.002
z2	0.0002042	2.327	0.04754	36.33	0.324	0.0002038	2.326	0.04763	36.36	0.312	0.0001928	5.132	0.05035	37.53	-0.032
z3	0.0002045	1.698	0.05200	22.74	0.315	0.0002041	1.703	0.05212	22.76	0.302	0.0001931	4.867	0.05508	23.78	-0.012
z5	0.0001972	3.766	0.03280	80.24	0.268	0.0001963	3.762	0.03294	80.34	0.243	0.0001852	7.184	0.03492	81.96	-0.066
z6	0.0002002	4.901	0.02030	196.57	0.402	0.0001987	4.777	0.02045	196.95	0.334	0.0001875	9.241	0.02167	200.39	-0.183
z7	0.0002204	3.331	0.05848	37.22	0.155	0.0002217	3.309	0.05812	37.16	0.171	0.0002108	4.556	0.06112	37.76	0.024
z8	0.0002036	2.771	0.02567	77.25	0.279	0.0002022	2.772	0.02584	77.38	0.232	0.0001910	7.074	0.02735	78.88	-0.083
z10	0.0002019	3.243	0.04477	50.40	0.184	0.0002003	3.272	0.04513	50.58	0.129	0.0001891	8.289	0.04780	52.52	-0.117
z11	0.0002099	2.831	0.04544	41.91	0.173	0.0002082	2.868	0.04582	42.07	0.117	0.0001971	7.937	0.04841	43.80	-0.097
z12	0.0002129	1.778	0.04237	27.58	0.206	0.0002126	1.783	0.04243	27.59	0.199	0.0002016	4.605	0.04474	28.37	-0.022
z13	0.0002052	1.133	0.04408	17.15	0.251	0.0002064	1.096	0.04383	17.12	0.280	0.0001955	3.279	0.04627	17.63	0.024
z14	0.0001988	5.857	0.01833	227.67	0.251	0.0001974	5.838	0.01846	227.94	0.204	0.0001864	10.227	0.01955	230.61	-0.130
z18	0.0002158	2.897	0.06473	30.19	0.189	0.0002169	2.882	0.06440	30.14	0.206	0.0002061	4.295	0.06778	30.80	0.025
z21	0.0002077	4.346	0.05633	57.67	0.299	0.0002090	4.351	0.05596	57.56	0.324	0.0001982	5.444	0.05902	58.62	0.084
JC21-76R-4															
z1	0.0002014	2.341	0.04223	40.00	0.356	0.0002009	2.339	0.04234	40.05	0.339	0.0001897	5.496	0.04483	41.29	-0.026
z2	0.0001978	1.665	0.03732	31.21	0.205	0.0001967	1.698	0.03753	31.28	0.164	0.0001854	6.280	0.03980	32.53	-0.065
z4	0.0002024	1.855	0.04545	30.03	0.347	0.0002027	1.854	0.04538	30.01	0.355	0.0001917	4.276	0.04799	30.86	0.014
z5	0.0002022	1.497	0.04571	24.57	0.368	0.0002023	1.496	0.04570	24.57	0.370	0.0001912	4.363	0.04835	25.44	0.004
z6	0.0002000	2.380	0.04334	40.12	0.308	0.0001992	2.381	0.04351	40.19	0.282	0.0001880	5.988	0.04612	41.53	-0.051
z7	0.0001993	2.955	0.04760	42.60	0.213	0.0002013	2.924	0.04711	42.51	0.245	0.0001904	4.172	0.04981	43.13	0.050
z8	0.0002004	3.204	0.05080	43.42	0.241	0.0002001	3.204	0.05086	43.44	0.236	0.0001891	5.771	0.05384	44.63	-0.030
z9	0.0001975	6.257	0.04929	90.73	0.291	0.0001974	6.255	0.04931	90.74	0.289	0.0001862	8.422	0.05226	92.97	-0.028
z16	0.0002046	6.124	0.05754	76.91	0.275	0.0002057	6.138	0.05720	76.77	0.297	0.0001949	7.246	0.06040	78.28	0.058

Supplementary Table S2 Continued

Dates																		
Uncorrected		Th-corrected (Th/U = 2.23 ± 0.31)				Th-corrected (D _{Th/U} = 0.25)				Th-corrected (D _{Th/U} = 0.85)								
²⁰⁶ Pb/g	2σ	²⁰⁷ Pb/g	2σ	²⁰⁷ Pb/g	2σ	²⁰⁶ Pb/g	2σ	²⁰⁷ Pb/g	2σ	²⁰⁶ Pb/g	2σ	²⁰⁷ Pb/g	2σ	²⁰⁶ Pb/g	2σ	²⁰⁷ Pb/g	2σ	
²³⁸ U	(abs)	²³⁵ U	(abs)	²⁰⁶ Pb	(abs)	²³⁸ U	(abs)	²⁰⁶ Pb	(abs)	²³⁸ U	(abs)	²⁰⁶ Pb	(abs)	²³⁸ U	(abs)	²⁰⁶ Pb	(abs)	
JC21-78R-5																		
z1	1.248	0.010	1.46	0.13	368	203	1.328	0.010	225	210	1.330	0.010	222	210	1.258	0.049	348	226
z2	1.231	0.033	1.36	0.50	232	831	1.316	0.031	77	863	1.314	0.031	81	863	1.243	0.064	211	870
z3	1.233	0.024	1.49	0.35	436	501	1.318	0.022	286	520	1.315	0.022	291	520	1.245	0.061	416	531
z5	1.183	0.051	0.91	0.73	-690	2211	1.271	0.048	-893	2323	1.265	0.048	-880	2320	1.194	0.086	-715	2283
z6	1.199	0.070	0.57	1.13	-2266	7831	1.290	0.063	-2572	8493	1.281	0.061	-2540	8442	1.208	0.112	-2299	8086
z7	1.347	0.048	1.80	0.68	663	792	1.420	0.047	548	813	1.429	0.047	534	814	1.359	0.062	644	812
z8	1.221	0.039	0.73	0.57	-1426	2512	1.312	0.036	-1667	2671	1.303	0.036	-1643	2661	1.231	0.087	-1453	2593
z10	1.209	0.044	1.26	0.64	109	1182	1.302	0.042	-68	1231	1.291	0.042	-49	1231	1.219	0.101	89	1245
z11	1.260	0.040	1.33	0.56	138	978	1.353	0.038	-32	1016	1.342	0.038	-12	1016	1.270	0.101	119	1032
z12	1.288	0.025	1.26	0.35	-48	667	1.372	0.024	-205	692	1.370	0.024	-201	691	1.300	0.060	-70	693
z13	1.248	0.015	1.27	0.22	35	407	1.323	0.015	-106	422	1.330	0.015	-120	422	1.260	0.041	12	424
z14	1.191	0.080	0.51	1.17	-2696	10117	1.282	0.075	-3038	11072	1.273	0.074	-3004	10990	1.202	0.123	-2736	10388
z18	1.316	0.041	1.95	0.60	882	619	1.391	0.040	766	636	1.398	0.040	755	636	1.328	0.057	862	639
z21	1.265	0.061	1.64	0.96	589	1239	1.338	0.058	465	1278	1.347	0.059	451	1278	1.278	0.070	568	1276
JC21-76R-4																		
z1	1.213	0.033	1.19	0.48	-44	964	1.298	0.030	-213	1005	1.295	0.030	-206	1005	1.223	0.067	-65	1008
z2	1.186	0.022	1.03	0.33	-343	800	1.275	0.021	-534	837	1.268	0.022	-518	836	1.195	0.075	-364	842
z4	1.224	0.026	1.29	0.39	121	701	1.305	0.024	-31	728	1.306	0.024	-35	728	1.235	0.053	99	730
z5	1.222	0.021	1.29	0.32	137	572	1.304	0.020	-18	594	1.304	0.020	-18	594	1.232	0.054	116	600
z6	1.202	0.033	1.21	0.49	23	955	1.289	0.031	-148	995	1.284	0.031	-138	995	1.212	0.073	4	1000
z7	1.215	0.039	1.33	0.57	209	980	1.284	0.038	79	1012	1.298	0.038	55	1014	1.227	0.051	186	1004
z8	1.208	0.044	1.42	0.63	385	967	1.292	0.041	232	1002	1.290	0.041	235	1002	1.219	0.070	364	1006
z9	1.190	0.085	1.36	1.26	316	2044	1.273	0.080	161	2122	1.272	0.080	162	2122	1.200	0.101	297	2122
z16	1.244	0.085	1.65	1.29	639	1638	1.319	0.081	512	1690	1.326	0.081	499	1691	1.256	0.091	618	1690

Supplementary Table S3 New and recalculated single grain ID-TIMS U-Pb zircon data from the Vema lithospheric section

	Composition				Isotopic Ratios								
	Pb*/ ^a	Pb*/ ^b	Pbc ^b	Th/ ^c	Uncorrected								
					²⁰⁶ Pb/ ^d	²⁰⁸ Pb/ ^e	²⁰⁶ Pb*/ ^e	2σ	²⁰⁷ Pb*/ ^e	2σ	²⁰⁷ Pb*/ ^e	2σ	corr. ^f
Pbc	(pg)	(pg)	U	²⁰⁴ Pb	²⁰⁶ Pb	²³⁸ U	(% err)	²³⁵ U	(% err)	²⁰⁶ Pb*	(% err)	coef.	
DR10-005													
z3	0.42	0.66	1.56	0.467	44.5	0.15035	0.0020897	2.744	0.01454	34.59	0.05047	34.18	0.185
z4	9.71	3.66	0.38	0.353	630.9	0.11371	0.0020617	0.142	0.01344	1.76	0.04729	1.72	0.263
z5	1.52	1.07	0.70	0.307	116.0	0.09911	0.0020847	0.764	0.01366	10.32	0.04751	10.18	0.223
z6	3.00	1.01	0.34	0.310	210.7	0.10005	0.0020597	0.437	0.01284	6.25	0.04522	6.10	0.368
z8	20.15	8.78	0.44	0.341	1293.7	0.10999	0.0020643	0.094	0.01348	0.83	0.04737	0.81	0.307
z10	2.25	0.77	0.34	0.402	158.1	0.12959	0.0020713	0.616	0.01402	7.85	0.04910	7.64	0.374
z11	1.48	0.65	0.44	0.335	112.2	0.10804	0.0020686	0.879	0.01466	10.99	0.05140	10.69	0.370
z12	1.10	0.48	0.44	0.316	88.9	0.10178	0.0020602	1.068	0.01217	15.98	0.04286	15.73	0.261
z14 ^h	6.34	2.18	0.34	0.327	421.9	0.10540	0.0020696	0.281	0.01298	3.51	0.04547	3.39	0.446
z15 ^h	10.38	3.37	0.32	0.335	676.7	0.10802	0.0020686	0.130	0.01336	1.64	0.04683	1.61	0.265
z16 ^h	6.42	1.92	0.30	0.386	419.8	0.12449	0.0020709	0.278	0.01347	3.90	0.04718	3.74	0.601
z17 ^h	1.49	0.80	0.54	0.365	112.6	0.11776	0.0020703	0.805	0.01340	10.94	0.04693	10.77	0.250
z18 ^h	1.88	0.55	0.29	0.348	137.2	0.11213	0.0020719	0.659	0.01361	8.82	0.04765	8.65	0.297
DR10-007													
z2	4.05	1.55	0.38	0.401	270.9	0.12938	0.0020612	0.325	0.01339	4.36	0.04711	4.26	0.352
z3	4.38	1.77	0.40	0.308	298.3	0.09941	0.0020603	0.311	0.01380	4.04	0.04858	3.92	0.406
z7	1.70	0.67	0.40	0.419	124.0	0.13495	0.0020650	0.779	0.01328	10.79	0.04666	10.52	0.373
z8	1.29	0.95	0.74	0.394	98.9	0.12692	0.0020788	0.973	0.01414	12.76	0.04935	12.47	0.328
z12	1.03	0.51	0.49	0.266	85.5	0.08563	0.0020495	1.122	0.01200	17.28	0.04247	17.02	0.263
z13	0.83	0.44	0.53	0.378	70.4	0.12187	0.0020474	1.532	0.01281	22.36	0.04539	21.88	0.349
z16	4.84	2.87	0.59	0.437	316.7	0.14077	0.0020516	0.284	0.01348	3.77	0.04764	3.68	0.337
VE2-3													
z1	5.13	2.21	0.43	0.281	349.1	0.09066	0.0021051	0.256	0.01374	3.30	0.04734	3.22	0.339
z2	8.93	3.33	0.37	0.331	585.3	0.10679	0.0021037	0.156	0.01383	1.91	0.04767	1.86	0.337
z4	23.76	8.52	0.36	0.428	1485.6	0.13785	0.0021046	0.086	0.01390	0.76	0.04790	0.74	0.330
z6	2.66	1.08	0.41	0.367	185.9	0.11828	0.0021147	0.487	0.01385	6.36	0.04750	6.22	0.315
z8	0.72	0.76	1.05	0.443	63.1	0.14284	0.0021211	1.644	0.01448	21.32	0.04950	21.00	0.229
z9	1.43	2.34	1.63	0.365	108.7	0.11773	0.0020979	0.851	0.01278	12.21	0.04418	12.02	0.257
z10	1.42	1.03	0.73	0.336	108.6	0.10840	0.0020915	0.845	0.01265	12.70	0.04386	12.49	0.281
z12	3.43	1.09	0.32	0.394	232.4	0.12685	0.0021044	0.396	0.01353	5.28	0.04665	5.16	0.347

Supplementary Table S3 Continued

	Dates														
	Th-corrected (Th/U = 2.36 ± 0.30)					Uncorrected					Th-corrected (Th/U = 2.36 ± 0.30)				
	²⁰⁶ Pb*/ ^e	2σ	²⁰⁷ Pb*/ ^e	2σ	corr. ^f	²⁰⁶ Pb/ ^g	2σ	²⁰⁷ Pb/ ^g	2σ	²⁰⁷ Pb/ ^g	2σ	²⁰⁶ Pb/ ^g	2σ	²⁰⁷ Pb/ ^g	2σ
²³⁸ U	(% err)	²⁰⁶ Pb*	(% err)	coef.	²³⁸ U	(abs)	²³⁵ U	(abs)	²⁰⁶ Pb	(abs)	²³⁸ U	(abs)	²⁰⁶ Pb	(abs)	
DR10-005															
z3	0.0021033	2.714	0.05014	34.20	0.180	13.457	0.369	14.66	5.03	217	791	13.545	0.367	202	794
z4	0.0020762	0.141	0.04696	1.73	0.256	13.277	0.019	13.56	0.24	64	41	13.370	0.019	47	41
z5	0.0020995	0.755	0.04717	10.18	0.217	13.425	0.103	13.77	1.41	75	242	13.520	0.102	58	243
z6	0.0020744	0.431	0.04489	6.10	0.362	13.264	0.058	12.96	0.80	-44	148	13.359	0.058	-61	149
z8	0.0020788	0.095	0.04704	0.81	0.299	13.294	0.013	13.60	0.11	68	19	13.387	0.013	51	19
z10	0.0020854	0.608	0.04877	7.65	0.368	13.339	0.082	14.14	1.10	153	179	13.429	0.082	137	180
z11	0.0020832	0.867	0.05104	10.70	0.364	13.322	0.117	14.78	1.61	259	246	13.415	0.116	243	247
z12	0.0020749	1.054	0.04255	15.74	0.256	13.267	0.142	12.29	1.95	-176	392	13.362	0.141	-194	394
z14 ^h	0.0020842	0.278	0.04515	3.39	0.440	13.327	0.037	13.09	0.46	-30	82	13.422	0.037	-47	83
z15 ^h	0.0020832	0.130	0.04650	1.61	0.257	13.321	0.017	13.47	0.22	40	38	13.415	0.017	24	39
z16 ^h	0.0020851	0.274	0.04686	3.74	0.594	13.336	0.037	13.59	0.53	58	89	13.427	0.037	42	90
z17 ^h	0.0020847	0.795	0.04661	10.78	0.244	13.332	0.107	13.51	1.47	46	257	13.425	0.107	29	258
z18 ^h	0.0020864	0.650	0.04732	8.66	0.291	13.343	0.088	13.73	1.20	82	205	13.436	0.087	66	206
DR10-007															
z2	0.0020753	0.321	0.04679	4.26	0.345	13.274	0.043	13.50	0.58	55	102	13.364	0.043	38	102
z3	0.0020750	0.306	0.04824	3.92	0.400	13.268	0.041	13.92	0.56	128	92	13.363	0.041	111	93
z7	0.0020790	0.769	0.04634	10.53	0.367	13.298	0.104	13.40	1.44	32	252	13.388	0.103	15	253
z8	0.0020929	0.961	0.04901	12.48	0.323	13.387	0.130	14.26	1.81	164	292	13.478	0.129	148	293
z12	0.0020646	1.107	0.04216	17.03	0.257	13.198	0.148	12.11	2.08	-199	426	13.295	0.147	-217	428
z13	0.0020617	1.511	0.04508	21.89	0.342	13.185	0.202	12.93	2.87	-34	531	13.277	0.200	-51	533
z16	0.0020654	0.281	0.04732	3.68	0.330	13.212	0.038	13.59	0.51	82	87	13.301	0.037	66	88
VE2-3															
z1	0.0021200	0.253	0.04701	3.23	0.333	13.556	0.035	13.86	0.45	67	77	13.652	0.035	50	77
z2	0.0021184	0.154	0.04734	1.86	0.330	13.547	0.021	13.94	0.26	83	44	13.641	0.021	67	44
z4	0.0021185	0.087	0.04758	0.74	0.319	13.553	0.012	14.02	0.11	94	18	13.642	0.012	79	18
z6	0.0021290	0.481	0.04718	6.23	0.309	13.618	0.066	13.97	0.88	75	148	13.710	0.066	59	148
z8	0.0021349	1.626	0.04918	21.01	0.224	13.659	0.224	14.59	3.09	172	490	13.748	0.223	157	492
z9	0.0021123	0.841	0.04388	12.02	0.251	13.510	0.115	12.90	1.56	-100	295	13.602	0.114	-117	296
z10	0.0021061	0.834	0.04355	12.50	0.275	13.469	0.114	12.76	1.61	-119	308	13.563	0.113	-136	309
z12	0.0021185	0.391	0.04633	5.16	0.341	13.551	0.054	13.65	0.72	31	124	13.642	0.053	15	124

Supplementary Table S3 Continued

	Composition				Isotopic Ratios								
	Pb*/ ^a	Pb*/ ^b	Pbc ^b	Th/ ^c	Uncorrected								
					²⁰⁶ Pb/ ^d	²⁰⁸ Pb/ ^e	²⁰⁶ Pb*/ ^e	2σ	²⁰⁷ Pb*/ ^e	2σ	²⁰⁷ Pb*/ ^e	2σ	corr. ^f
Pbc	(pg)	(pg)	U	²⁰⁴ Pb	²⁰⁶ Pb	²³⁸ U	(% err)	²³⁵ U	(% err)	²⁰⁶ Pb*	(% err)	coef.	
VE2-5													
z3	1.82	0.76	0.42	0.384	132.3	0.12364	0.0020959	0.680	0.01360	9.39	0.04706	9.21	0.305
z4	1.11	1.51	1.35	0.411	87.5	0.13247	0.0021024	1.057	0.01440	13.59	0.04967	13.40	0.217
z5	3.87	1.55	0.40	0.340	263.8	0.10959	0.0021061	0.351	0.01376	5.19	0.04737	5.06	0.403
z6	1.72	1.03	0.60	0.365	126.4	0.11760	0.0020840	0.716	0.01436	9.26	0.04996	9.07	0.300
z7	0.49	0.65	1.34	0.397	48.9	0.12799	0.0020785	2.369	0.01311	33.21	0.04574	32.81	0.202
z8	1.25	1.39	1.11	0.279	99.3	0.08986	0.0020941	0.936	0.01363	12.57	0.04720	12.36	0.262
z10	2.26	1.57	0.70	0.355	160.7	0.11436	0.0020975	0.530	0.01395	6.92	0.04824	6.81	0.246
z13	2.45	1.28	0.52	0.330	174.3	0.10630	0.0020947	0.517	0.01308	7.63	0.04530	7.46	0.353
z15 ^h	1.50	0.65	0.44	0.318	113.9	0.10249	0.0020981	0.791	0.01380	10.64	0.04772	10.45	0.268
z16 ^h	1.51	0.59	0.39	0.333	115.0	0.10744	0.0021060	0.794	0.01258	11.97	0.04334	11.77	0.282
z17 ^h	2.22	1.14	0.51	0.357	158.7	0.11502	0.0020839	0.534	0.01306	7.57	0.04546	7.46	0.241
z18 ^h	0.98	0.45	0.46	0.346	80.7	0.11148	0.0020838	1.303	0.01309	19.92	0.04557	19.49	0.361
VE4-13													
z1	5.22	3.00	0.58	0.514	333.5	0.16548	0.0020420	0.260	0.01369	3.41	0.04863	3.34	0.308
z2	1.68	0.84	0.50	0.418	122.8	0.13470	0.0020501	0.724	0.01301	10.07	0.04603	9.91	0.260
z3	2.08	0.72	0.35	0.549	142.5	0.17683	0.0020430	0.651	0.01384	9.15	0.04914	8.93	0.360
z4	1.01	0.71	0.70	0.414	81.2	0.13334	0.0020486	1.290	0.01345	17.94	0.04761	17.50	0.372
z5	2.13	0.80	0.37	0.399	151.3	0.12873	0.0020640	0.568	0.01374	7.71	0.04827	7.57	0.274
z6	1.76	0.67	0.38	0.579	122.7	0.18635	0.0020473	0.747	0.01373	10.41	0.04862	10.18	0.337

^a Ratio of radiogenic to common Pb.

^b Total radiogenic Pb and common Pb (picograms).

^c Th/U ratio calculated from ²⁰⁸Pb/²⁰⁶Pb and the ²⁰⁶Pb/²³⁸U date of the sample.

^d Fractionation and spike corrected isotopic ratios.

^e Fractionation, spike, and blank corrected radiogenic isotope ratios. Laboratory blanks were corrected using ²⁰⁶Pb/²⁰⁴Pb = 18.638 ± 0.707, ²⁰⁷Pb/²⁰⁴Pb = 15.494 ± 0.449, ²⁰⁸Pb/²⁰⁴Pb = 37.748 ± 1.227.

^f Correlation coefficient of radiogenic ²⁰⁷Pb*/²³⁵U and ²⁰⁶Pb*/²³⁸U.

^g Dates (Ma) calculated using ²³⁸U/²³⁵U = 137.88, and decay constants of ²³⁸U = 1.5513 x 10⁻¹⁰ yr⁻¹ and ²³⁵U = 9.8485 x 10⁻¹⁰ yr⁻¹.

^h New analyses completed since the publication of Lissenberg (2009)

Supplementary Table S3 Continued

	Dates														
	Th-corrected (Th/U = 2.36 ± 0.30)					Uncorrected					Th-corrected (Th/U = 2.36 ± 0.30)				
	²⁰⁶ Pb*/ ^e	2σ	²⁰⁷ Pb*/ ^e	2σ	corr. ^f	²⁰⁶ Pb/ ^g	2σ	²⁰⁷ Pb/ ^g	2σ	²⁰⁷ Pb/ ^g	2σ	²⁰⁶ Pb/ ^g	2σ	²⁰⁷ Pb/ ^g	2σ
²³⁸ U	(% err)	²⁰⁶ Pb*	(% err)	coef.	²³⁸ U	(abs)	²³⁵ U	(abs)	²⁰⁶ Pb	(abs)	²³⁸ U	(abs)	²⁰⁶ Pb	(abs)	
VE2-5															
z3	0.0021101	0.672	0.04675	9.21	0.299	13.497	0.092	13.72	1.28	53	220	13.588	0.091	36	221
z4	0.0021164	1.045	0.04934	13.41	0.211	13.539	0.143	14.52	1.96	180	312	13.629	0.142	164	313
z5	0.0021207	0.346	0.04704	5.07	0.396	13.563	0.048	13.87	0.72	68	120	13.656	0.047	51	121
z6	0.0020984	0.706	0.04962	9.08	0.294	13.421	0.096	14.47	1.33	193	211	13.513	0.095	177	212
z7	0.0020927	2.341	0.04543	32.83	0.196	13.385	0.317	13.22	4.36	-16	793	13.476	0.315	-33	796
z8	0.0021091	0.924	0.04687	12.37	0.256	13.485	0.126	13.75	1.72	59	295	13.582	0.125	42	296
z10	0.0021120	0.523	0.04791	6.81	0.241	13.507	0.071	14.07	0.97	111	161	13.600	0.071	95	161
z13	0.0021093	0.510	0.04498	7.47	0.347	13.489	0.070	13.20	1.00	-40	181	13.583	0.069	-57	182
z15 ^h	0.0021128	0.781	0.04738	10.46	0.262	13.511	0.107	13.92	1.47	85	248	13.605	0.106	69	249
z16 ^h	0.0021206	0.783	0.04304	11.77	0.276	13.562	0.108	12.70	1.51	-148	292	13.656	0.107	-165	293
z17 ^h	0.0020984	0.528	0.04515	7.46	0.235	13.420	0.072	13.18	0.99	-31	181	13.513	0.071	-48	182
z18 ^h	0.0020983	1.284	0.04525	19.50	0.354	13.419	0.175	13.21	2.61	-25	472	13.512	0.173	-42	474
VE4-13															
z1	0.0020553	0.258	0.04832	3.34	0.301	13.150	0.034	13.81	0.47	130	79	13.235	0.034	115	79
z2	0.0020641	0.716	0.04571	9.92	0.254	13.202	0.096	13.13	1.31	-1	239	13.292	0.095	-17	240
z3	0.0020561	0.643	0.04883	8.94	0.352	13.157	0.086	13.96	1.27	155	209	13.241	0.085	140	210
z4	0.0020627	1.272	0.04729	17.51	0.366	13.193	0.170	13.57	2.42	80	415	13.283	0.169	64	417
z5	0.0020782	0.561	0.04795	7.58	0.267	13.292	0.075	13.85	1.06	113	179	13.383	0.075	97	179
z6	0.0020601	0.738	0.04832	10.19	0.330	13.184	0.098	13.84	1.43	130	240	13.267	0.098	115	240